2016

Organic Rankine Cycle Control using Neural Networks and Variable Structure Control

Badkoubeh Hezaveh, Babak

UNIVERSITY OF CALGARY

Organic Rankine Cycle Control using Neural Networks and Variable Structure Control

by

Babak Badkoubeh Hezaveh

A THESIS

SUBMITTED TO THE FACULTY OF GRADUATE STUDIES

IN PARTIAL FULFILLMENT OF THE REQUIREMENTS FOR THE

DEGREE OF MASTER OF SCIENCE

GRADUATE PROGRAM IN MECHANICAL AND MANUFACTURING ENGINEERING

CALGARY, ALBERTA

September, 2016

Abstract

This research work proposes an adaptive optimal Lyapunov control for a Trans-critical Organic Rankine Cycle (TORC) to address disturbance rejection problem. TORC is a thermodynamic cycle for converting low temperature heat into electrical power where the system operates with an organic fluid with low boiling temperature at supercritical or trans-critical conditions. This thermodynamic cycle is similar to the traditional steam Rankine cycle, but it is capable of recovering low grade heat into useful power. The control-oriented challenge of utilizing this system at nominal efficiency is that low grade heat resources have a fluctuating nature which does not allow the heat recovery system operates at nominal operating conditions. In this regards, a control-oriented nonlinear model of TORC system is developed, and an Adaptive Variable Structure Control (AVSC) using Cerebellar Model Articulation Controller (CMAC) neural networks is proposed to maintain the system at nominal operating conditions while rejecting the disturbances. The variable structure control is a well known robust control strategy suitable for this application where CMAC neural network method integrates into the control such that the final control is not only robust but also adaptive to the disturbances.

Acknowledgements

First of all, I would like to thank my thesis advisor, Dr. Jeff Pieper of Mechanical Engineering Department, University of Calgary for his continuous support, patience, and motivation during my M.Sc. study. It has been an honor to be one of his students. I would also like to appreciate all the efforts by Dr. Chris Macnab of Electrical Engineering Department, University of Calgary as my co-supervisor for his valuable suggestions and critiques, which led to having a comprehensive range of feedback.

I would like to thank my committee members, Dr. Peter Goldsmith and Qiao Sun from department of Mechanical Engineering, University of Calgary, and Dr. Milana Trifkovic from department of Chemical Engineering, University of Calgary, for their time on reviewing my thesis and attending my defense session, and also for their constructive suggestions. Additionally, I would like to acknowledge the financial support of Genalta Power Company.

I enjoyed every moment of being with my dear officemates, Jilan Samiuddin and Rachael L'Orsa, at our shared office, and thank them for providing a friendly atmosphere throughout these two years research work.

Last but not least, I must express my deepest gratitude to my parents and to my brother who has always been there and encouraged me throughout all good and challenging days of my life. This accomplishment would not have been possible without their spiritual support.

Table of Contents

List of Figures and Illustrations

List of Symbols, Abbreviations and Nomenclature

Symbol	Definition
ORC	Organic Rankine Cycle
TORC	Trans-critical Organic Rankine Cycle
SORC	Sub-critical Organic Rankine Cycle
MB-model	Moving Boundary Model
CMAC	Cerebellar Model Articulation Controller
VSC	Variable Structure Control
WHR	Waste Heat Recovery
VSC	Variable Structure Control
AVSC	Adaptive Variable Structure Control
CV	Controlled Variable
MV	Manipulated Variable
MIMO	Multi-inputs Multi-outputs
SISO	Single-input Single-output

Chapter 1

INTRODUCTION

Energy plays an essential role in all aspect of our life so that it is our responsibility to protect the energy resources and harness these resources more efficiently. The rate of economic development in the world over the last century was entangled with the rate of energy consumption. This growth of energy consumption has been sadly involved with more consumption of fossil fuels and emission of more carbon dioxide that results in increasing atmospheric pollution, global warming and so many dramatic consequences on the environments. According to the European Commission 2050 low-carbon economy road-map [1], by 2050 EU should cut carbon emissions to 80% below 1990 levels and the milestones are 40% by 2030 and 60% by 2040 reduction in carbon emission below 1990 levels. Also, Alberta provincial government in Canada has recently set up a regulation on reduction of emission of greenhouse gases. This is facility that emits more than 100,000 tonnes greenhouse gases must reduce their emission to 20% by 2017 and a levy on carbon has been also imposed as a cost-effective way of reducing carbon emissions [2].

Sustainable use of energy and efficient consumption are the best way of preserving natural resources for next generations. From the engineering perspective, the sustainable development of energy resources includes improvement of machine efficiency to minimize waste energy. The waste energy is usually in the form of thermal energy which is discharged into the environment through chimneys of factories, exhaust gas, or many other ways. However, the waste heat can be recovered into a useful type of energy such as electricity by a thermal converter system. The conversion of thermal energy into electricity has been well developed and utilized for a long time since the heat engine was invented in 18th century. Eventually, the thermodynamics law continued to develop gradually such as Carnot's theorem, entropy principle or second law of thermodynamics.

Thermodynamics as a major branch of physical science continues developing in collaboration with other disciplines to design and build advanced thermal systems.

After building a complex system, a perpetual challenge is how to make efficient use of the system. To tackle such issue, the disciple of Control Systems is a must to get most out of the system such that the applied control makes desired behaviors in the system. As a general statement, the more complex system, the more advanced control system is needed. The Control System is relatively new engineering field which received significant attention during 20th century due to the rapid technology advancement . This engineering discipline embraces a wide range of applications, from a household washing machine to a spacecraft design. This field of engineering is to thoroughly understand the behavior of a system in the language of mathematics, then to design a controller towards the desired behavior [3].

As a sustainable development example, a complex thermodynamic system called Organic Rankine Cycle will be introduced, then its applications and its types will be explained in this chapter. To make the best use of this system, there are quite a few control-oriented challenges such as disturbances and model uncertainties. Thus, the challenges will be pointed out, and finally, a solution for them will be proposed. Control system has shown promising contribution to improvement of power plants net power output that is 2-4% greater power output [3]

1.1 Organic Rankine Cycle

Organic Rankine Cycle (ORC) system is a low temperature thermal power plant which is capable of converting low quality heat into electricity. The ORC system is conceptually identical to the traditional steam Rankine cycle shown in figure 1.1 whereas the working fluid is different. The working fluid in the ORC system is an organic fluid with low boiling temperature which contributes

to being capable of converting low temperature heat resources into electricity. Similarly, the ORC system comprises evaporator, condenser, turbine expander and pump such that the ideal Rankine cycle consists of the following four processes:

1-2 Isentropic compression in the pump,

2-3 Constant pressure heat addition in the evaporator,

3-4 Isentropic expansion in the turbine expander,

4-1 Constant pressure heat rejection in the condenser.

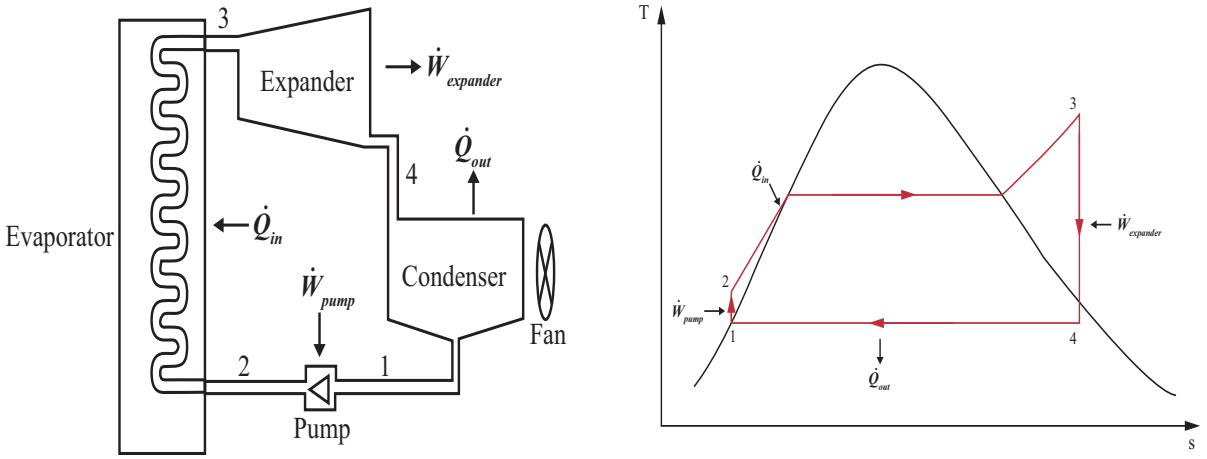

(a) components of an ideal Rankine cycle (b) T-s diagram of an ideal Rankine cycle

Figure 1.1: conceptual scheme of an ideal Rankine cycle

Figure 1.1 shows the consisting components and the four processes of an ideal Rankine cycle. Working fluid enters the pump at state 1 as a saturated liquid, then the pump consumes energy and compresses the working fluid to the operating pressure of the evaporator, state 2. The working fluid temperature increases through absorbing heat in the evaporator essential at a constant pressure where the working fluid reaches state 3. Then, it enters the turbine expander where it expands isentropically and produces mechanical energy which is coupled to an electric generator. Through this process, pressure and temperature of the working fluid drop to state 4 where it enters the condenser for heat rejection. Through rejecting the heat to ambient, the working fluid is condensed at

constant pressure to state 1 where the cycle has started. Furthermore, the area under the process curve 2-3 in the T-s diagram represents the heat transferred to the working fluid in the evaporator. The area under the process curve 4-1 in the T-s diagram represents the heat rejected in the condenser. Therefore, the difference between this two area where enclosed by the cycle curve is the produced net work.

On the other hand, the actual cycle differs from the ideal one due to irreversibilities in the consisting components. Fluid friction and heat loss to the ambient are two sources of irreversibilities. The fluid friction results in pressure drop in the evaporator, the condenser and the pipeline between components. The heat loss from the working fluid to the ambient occurs as the working fluid flows through the components. Hence, these sources of irreversibilities contribute to a decrease in cycle efficiency. Increasing the Rankine cycle net power output has always been an engineering issue so that various approaches have been proposed to tackle this issue such as increasing the operating pressure of the evaporator such that it automatically raises the temperature at which heat is transferred to the working fluid. In this work, the focus is on efficiency improvement and net power output enhancement of an Organic Rankine cycle under trans-critical pressure and temperature.

The operating pressure of the evaporators has gradually increased over the years. Nowadays, there are many modern power plants operate at trans-critical pressure resulting in higher thermal efficiency [4]. Figure1.2 illustrates the T-s diagram of a Trans-critical Rankine cycle. Beside trans-critical approach for efficiency improvement, the selection of working fluid is another mean of increasing the thermal efficiency in agreement with heat source temperature. Studies have shown when the heat source is classified as low-grade ($60^\circ - 220^\circ$) or as medium-grade ($220^\circ - 450^\circ$), selection of appropriate working fluid plays an important role to achieve high efficiency. Choice of organic fluids with lower latent heat and lower pinch points shows better performance than the water in low temperature applications [5, 6] so that ORC systems are better off with utilizing low

to medium grade heat resources. In particular, this work addresses efficiency enhancement of a Trans-critical Organic Rankine Cycle (TORC) where it is more cost-effective than sub-critical Organic Rankine Cycle (SORC) [7].

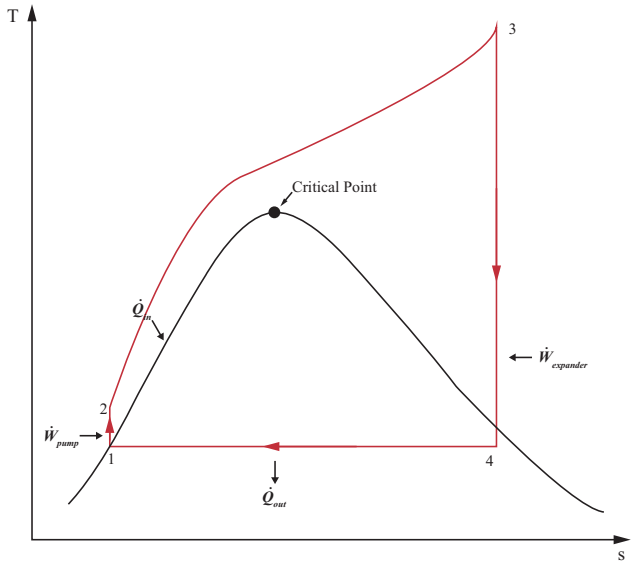

Figure 1.2: T-s diagram of a Trans-critical Rankine cycle

There are essentially two stages to increase the efficiency of TORC systems, design stage and control stage. The design phase consists of the selection of the working fluid [8, 9, 10]; component selection and integration into ORC system [11, 12]; parameter optimization [7]; and process integration of the system [13]. After the design stage, control stage consists of developing a control system to shape the transient behavior of the system to achieve a desired behavior such that the system can reach the theoretical performance of the design stage.

Conversion of low temperature heat resources into useful power provide a broad application for ORC systems such as geothermal energy [14], solar thermal energy [15, 14], biomass product [8] and waste heat recovery (WHR). Figure 1.3 illustrates how ORC systems can be utilized for waste heat recovery or solar energy applications. Another ORC system application for WHR is in heavy-duty vehicles such that reducing heat loss has the most opportunity for overall efficiency

improvement of the vehicle. Although ORC systems are associated with low efficiency (8%-12%) [16], this small scale system are relatively easy to manufacture their components. Also, Honda Motor has built and tested Rankine cycle co-generation unit on their hybrid vehicle by recovering the waste heat of the exhaust gas to recharge the battery pack. The test has revealed that the use of WHR unit has improved the engine efficiency by 3.8% in 100 kph constant-speed driving.

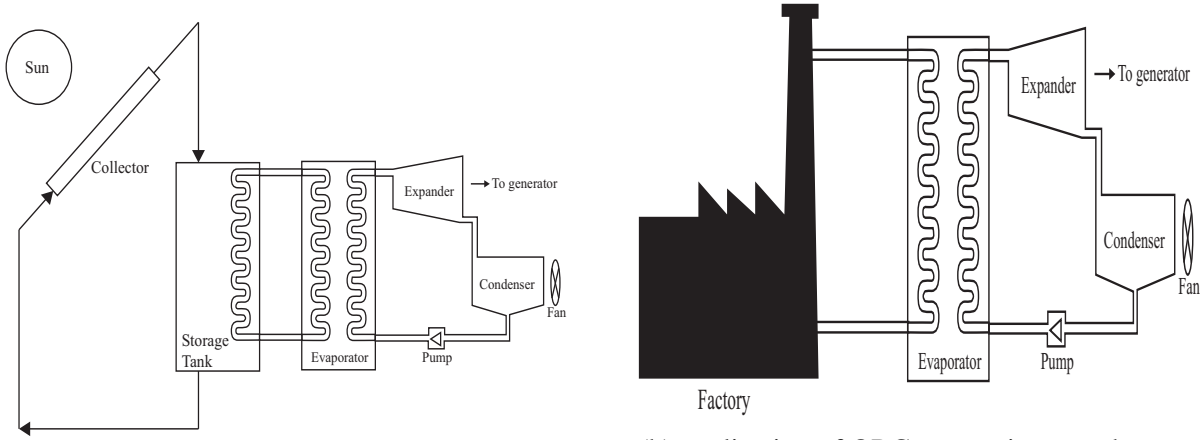

(a) application of ORC system in solar energy

(b) application of ORC system in waste heat recovery

Figure 1.3: two sample applications of ORC system in low-grade heat resources

In this work, the topics which will be covered comprise control-oriented modeling of ORC systems including SORC and TORC, control system design including controller design and state estimate design.

1.2 Control-oriented ORC Model

This section focuses on the methodology of an ORC dynamic modeling suitable for model-based control purposes. A control-oriented model is based on approaches with trade-offs between accuracy and low computation. In other words, this model is accurate enough to capture dominant modes of a system while it is not computationally expensive. Hence, to develop a control-oriented model of a system where the system consists of different components, first, the components must be classified into a fast dynamic and a slow dynamic categories such that a slow dynamic components have a time constant at least 10 times longer than fast dynamic components [17]. This

reduces the complexity and ill-conditioning level of the model [18]. Then, for control purposes, dynamic models of the slow dynamic components are derived whereas static models of the fast dynamic components are considered. Finally, interconnections of the component models build the overall model of the system. ORC systems comprise sub-systems including heat exchangers, pump, and turbine expander so that each component must be modeled separately. Given the fast and slow dynamic classification, static models of pump and turbine expander will be developed due to their fast dynamic characteristics , and dynamic model of heat exchangers will be derived due to their slow dynamic characteristics [19, 20].

In modeling of ORC systems, the challenging part is developing the dynamic model of heat exchangers for control purposes. In this regards, thermodynamic laws including conservation of mass and conservation of energy are used to model the heat exchangers. Conservation of momentum is not considered in this work since pressure drop in heat exchangers are neglected. Dynamic models of heat exchangers can be classified into three categories: lumped parameters models, moving boundary models and discretization of PDE models.The discretization of PDE models are close to the truth model, but they have a high level of complexity so that they are not suitable for control purposes [21]. The most appropriate control-oriented model is the moving boundary model (MB-model). However, if the working fluid is in trans-critical condition MB-model cannot be utilized since there is not phase boundary in a trans-critical fluid. Also, where the accuracy does not matter, lumped parameters model can be used. For instance, preheater or recuperator in a Rankine cycle can be modeled by a lumped parameters model.

In this work, the MB-model is based on Jensen's Ph.D. thesis in 2003 with focus on dynamic modeling of evaporators [22, 23] although MB-model is known as well-developed old model for heat exchangers. The MB-model has been widely used including vapor compression cycle for HVAC systems such as He *et al.* [24, 25] or Rasmussen [26], and Rankine cycle such as

[21, 19, 27, 28]. Furthermore, in the control-oriented modeling of trans-critical heat exchangers, Rasmussen used a 13th order dynamic model consisting of a single region model for a trans-critical gas cooler and a lumped parameter model for a preheater in a trans-critical vapor compression cycle [26]. Note that the vapor compression cycle has a similar structure to Rankine cycle, but Rankine cycle has an inverse functionality where it is utilized as power generation cycle. Similarly, in this work, a 13th order dynamic model is developed for TORC system.

Another modeling challenge is the estimation of the model parameters such as heat transfer coefficients, pump or expander parameters. To estimate heat transfer coefficient for single-phase flow in a circular tube is calculated by Gnielinski's correlation where Nussel number is calculated using Dittus-Boelter equation referred in [29]. For pump and expander semi-empirical static model is used. Thus, dynamic MB-model for heat exchangers combined with static models of pump and expander provides a ground for control system design in general. Similarly, Wei *et al.* [21] used this approach for WHR ORC model where methodology of selection of thermodynamic state variables was explained according to Duhem's theorem which states that the equilibrium state of a system is completely determined by two independent variables when the initial masses are known [21]. Therefore, if the conservation of momentum is neglected, there is no need for a third independent variable to determine the equilibrium state of the system. Ultimately, choosing two intensive variables among the set of $\left\{ P \quad h \quad \rho \quad u \quad s \right\}$ contributes to 10 possible combinations. In this work, the pair of $\left\{ P \quad h \right\}$ is selected as state variables in modeling section as this pair leads to relatively robust model [23]. Similarly, Quoilin *et al.* [30, 31] developed a dynamic model for WHR SORC system using a scroll expander where the same modeling approach is utilized for control purposes.Furthermore, Esposito *et al.* [28] followed the same modeling approach to design a nonlinear model predictive control for WHR SORC in automotive engines. Finally, Zhang *et al.* [32, 33, 20] used this control-oriented modeling approach for SORC system.

1.3 Control of ORC systems

Heat resources are often unsteady or transient, which causes a lower performance than the nominal one. Therefore, an advanced control system must be designed to maintain the ORC system at maximum performance. Now that, there are control-oriented challenges which must be taken into account including disturbance imposed by the transient behavior of the heat source. The disturbance causes the system deviates from the optimal operating conditions results in decreasing the system efficiency. Thus, the first control objective is to track the optimal set-point while the disturbance is affecting the system through the fluctuation of heat source temperature. In ORC systems, not only efficiency is of high importance but safety also is a key factor. The safety factor is to maintain the proportion of liquid and vapor in the heat exchangers in an acceptable range, otherwise it causes stalling or temperature shocks to the components and damaging the system. For instance, if an excessive wet flow enters into the turbine expander, it results in bending damages in the turbine's blades. Ultimately, all these challenges highlight the importance of a control system to guarantee safety and performance.

Quoilin *et al.* [31] proposed an optimal control strategy in SISO control architecture for an SORC where a static model was utilized to derive the optimal evaporating temperature and superheating over a wide range of heat source and heat sink conditions. Expander rotation speed and pump capacity were the manipulated variables to control superheating and evaporating temperature as two important variables in SORC systems. Furthermore, two PI controllers were used to track the calculated optimal set-point. In this SISO strategy, pump capacity controlled the evaporating temperature which is a function of high pressure, and expander speed controlled the superheating.

Due to the better performance that multivariable control scheme, MIMO, exhibits in ORC applications, they have got the attention of researchers in control of ORC systems [27]. Zhang *et al* [19] developed a dynamic model with moving boundaries for the evaporator and the condenser.

Afterward, a linear state space model was derived for control system design purposes. Regarding the overall system efficiency, the degree of superheating in the evaporator and the condenser outlet temperatures were regulated. A linear quadratic regulator coupled to a PI (proportional-integral) controller have been designed and simulated for set point changes in the power output and the throttle valve pressure (i.e., pressure at the entrance of the expander) as well as the superheating and condenser temperatures. The PI controller maintained the condenser outlet temperature at the desired level. Likewise, disturbance rejection scenarios were investigated associated with hot gas stream velocity variation and throttle valve dynamics. Zhang *et al* [32] extended the previous work. He developed an extended observer to have an accurate state estimate for the system.

A dynamic model for a waste heat recovery system introduced by Zhang *et al.* [33] is based on an ORC system with R245fa as the working fluid. Then, the first principles dynamic model was converted to a CARIMA (controlled auto-regressive integrated moving average) model for use in a model predictive control scheme. The system power output, the evaporator pressure, the superheating temperature, and the condenser temperature were the controlled variables in the multivariable control scheme. In order to control these variables, the pump and expander rotating speeds and the air flow in the condenser were utilized. Implementing a constrained generalized predictive controller resulted in having the rejection of disturbances and following the set-point in an efficient manner. Zhang *et al.* [20] proposed a constrained generalized predictive controller that took into account bounds on both the manipulated and controlled variables as well as the rate of change for the manipulated variables. The performance of the controller has been assessed for disturbances in the temperature and the flow rate of the heat source stream. Power output was maintained at the desired level despite the disturbances. Furthermore, the controller could successfully track the set-point changes for the evaporator pressure, the superheating temperature, and the condenser temperature.

Recently, Hou *et al.* [34] introduced a minimum variance controller with real-time parameter estimation for a CARMA (controlled auto-regressive moving average) model. A recursive least squares technique was implemented for the parameter estimation. But, the proposed control scheme does not take into account a model for the stochastic disturbances in the system. Since uncertainties play a major role in the performance of the ORC system; consequently, to monitor the changes in the dynamic features on-line the measurements from the process should be used. Moreover, the inherent nonlinearities in the system may lead to having a significant inaccuracy in the predictions from linearized process models. To do so, Zhang *et al.* [19] introduced a state extended observer for the on-line update of states and model parameters. Then, the updated model is used in a linear quadratic regulator with a PI controller for the plant control.

In conclusion, MIMO control architecture due to the incorporation of the coupling between multiple inputs and outputs improves the transient behavior of the ORC system in comparison with SISO control architecture [31]. Relative Gain Array (RGA) analysis [17] shows that there is a considerable coupling between the control variables- the evaporator outlet temperature and high pressure. Note that sub-cooling is the other important variable in ORC, but according to RGA analysis, this variable can be controlled by fan rotation speed with a separate PI controller.

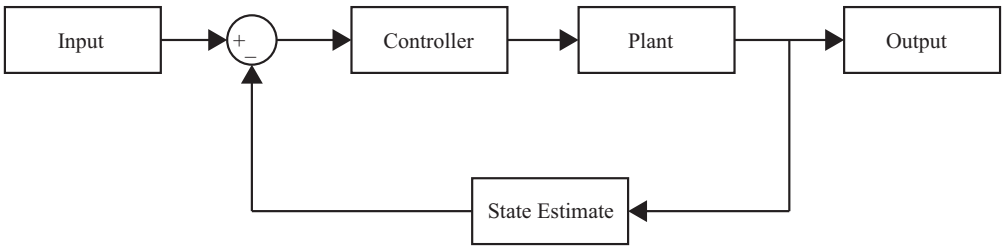

Figure 1.4: closed-loop control architecture principle

Figure 1.4 illustrates the principle of a closed-loop control architecture in block diagrams where the controller uses state error to generate control input of the plant. The state estimator is designed to provide all system states by output measurements. In this work, the control variables are high pressure and evaporator outlet temperature. The control inputs are the pump rotation speed and turbine expander rotation speed. Sources of disturbances to ORC system are the fluctuation of heat

source temperature and fluctuation of ambient temperature. Also, due to a negligible frequency of changes of ambient temperature in comparison with heat source temperature, ambient temperature is assumed constant in this work. For the control design, an optimal control strategy inspired from optimal sliding mode control is designed where it guarantees robustness characteristic of the controlled. Then, the optimal controller combined with CMAC neural networks to make the controller adaptive to deterministic and indeterministic uncertainties and disturbances.

1.4 Motivation and Objective

This work concentrates on semi-model based control of a TORC system since there is a significant uncertainty in TORC model. Moreover, fluctuation of heat source temperature is a considerable indeterministic disturbance into the TORC system. To the extent of authors' knowledge, there are not any accurate control-oriented models for Trans-critical ORC systems so far. To sum up, the control-oriented challenges of controlling TORCs are as follows:

- *Model Uncertainties*: inaccuracy of thermodynamic equation of states (EoS) in trans-critical conditions resulted in parameter uncertainties, unmodeled dynamics, neglect of nonlinear terms in linear model, linearization process;
- *Disturbance*: fluctuation of heat source as a primary contributing factor in model parameters change (variation of ambient temperature is negligible);
- *Sensitivity*: high level of sensitivity in high-pressure channel;
- *Coupling*: high degree of coupling among control variables (high pressure and evaporator outlet temperature) and control inputs (pump rotation speed and expander rotation speed);
- *Constraints*: constraints on control inputs and state variables concerning safety and efficiency;

- *Unmeasurable system state*: existence of some unmeasurable system states including phase boundaries and heat exchanger wall temperatures;
- *Measurement noise*: existence of measurement noise in system outputs.

Accordingly, the control strategy must address all of these challenges in TORC system. Therefore, the controller must have the following characteristic to tackle such issues:

- *Robustness*: to overcome uncertainties and disturbances;
- *Adaptability*: to adjust to the model parameters change due to the fluctuation of heat source;
- *Semi-model base*: to not fully rely on uncertain model;
- *Optimality*: to penalize the control in case of approaching the constraints;
- *MIMO control*: to consider the control variables and control inputs couplings;
- *State observation*: to estimate unmeasurable state variables.

In addition to these objectives, the author is aiming for proposing a means of controlling uncertain systems in general.

1.5 Treatment Approach and Contributions

To address all of the challenges mentioned above, we propose an adaptive optimal variable structure control such that a variable control structure is integrated with CMAC neural networks in which a Kalman filter [35] optimal state observer provides state estimate while rejecting the sensor noise. The proposed control is an adaptive robust semi-model based MIMO control combined with Kalman filter estimator chosen as a suitable control approach for set-point tracking and disturbance rejection. This enables the closed-loop system to follow optimal operating conditions while canceling out the effect of uncertainties as a result of adaptation to the level of disturbances through online training of neural networks. To sum up, the contribution of this work consists of:

- introducing a control-oriented model for a TORC plant through developing dynamic models of the heat exchangers and static models of the pump and the turbine expander as well as estimation of heat transfer coefficient for different thermodynamic conditions;

- proposing a novel control methodology through the integration of CMAC neural networks into an optimal variable structure control to design an adaptive optimal robust control which is a combination of the classical control discipline with the intelligent control discipline for set-point tracking and disturbance rejection of TORC;

- conducting stability analysis of the adaptive VSC design using Lyapunov stability theory to derive the adaptation laws so that the system can adapt to the model parameters change due to external disturbances, and nonlinearity imposed by set-point changes from the nominal operating conditions;

- integration of a Kalman filter as an optimal state observer into the adaptive VSC design to estimate unmeasurable system states and to enhance the practicality of the designed controller.

Chapter 2

MODELING OF ORGANIC RANKINE CYCLE

This chapter shows the modeling methodology of Organic Rankine Cycles in general such that each component of ORC system will be modeled separately, then all models will be combined into a global model representing the final model of an ORC system. Furthermore, the last section in this chapter will show how to model each type of ORC systems, Sub-critical ORC (SORC) and Trans-critical ORC (TORC). It is noted that in this work, our focus is on TORC system as the TORC control design is more challenging than SORC control because there is more model uncertainties are involved in TORC model.

2.1 Heat Exchanger Dynamic Models

This section describes different heat exchanger models which will be utilized to derive the dynamic model of the ORC system. In general, heat exchangers are the essential part of a thermodynamic system as they can be utilized as an evaporator, condenser or recuperator. Also, they have relatively slow dynamic nature in comparison with the other components of the thermodynamic system such as the pump or turbine expander. From the control design viewpoint, slow dynamic elements of a system capture the dominant modes of the system. Thus, for a model-based controller, control-oriented dynamic model of heat exchangers must be derived. In control-oriented models, there is a trade-off between accuracy and complexity of the model which means the model must be accurate while simple enough for control design purposes. Given this goal, various control-oriented heat exchanger models will be explained in this section. Also, in this section, there are some assumptions made for the heat exchanger models as follow:

1. long, thin and horizontal tube,

2. one-dimensional flow,

3. negligible kinetic energy,

4. negligible gravitational forces

5. constant cross-sectional area of the heat exchanger tubes,

6. negligible axial heat conduction in the working fluid and pipe wall,

7. cross flow heat exchangers

8. negligible pressure drop along the heat exchanger tubes so that the momentum balance is superfluous.

2.1.1 Moving Boundary Model

One of the best control-oriented heat exchanger models is moving boundary (MB) model because MB model captures the essential dynamic behavior of a heat exchanger through only 7 state variables in general. In other words, this 7^{th} order model embraces accuracy and simplicity features, that is appropriate for control system design. On the other hand, this model can only be used for sub-critical thermodynamic conditions as the boundary of each phase of the working fluid can be identified only in sub-critical conditions.

Figure (2.1) illustrates a conceptual scheme of a general MB model of a heat exchanger. The distinct physical behavior among the sub-cooled region, two-phase region, and superheated region in the two-phase heat exchangers motivates to derive MB-model. For instance, the heat transfer coefficient may differ significantly from the superheated region to the two-phase region, but with a good approximation, it is constant in each region so that the heat transfer coefficient in each region is independent of the spatial axis.

According to the idea of MB-model, the heat exchanger is divided into three regions, sub-cooled, two-phase and superheated such that the length of each region is dynamically tracked. Each

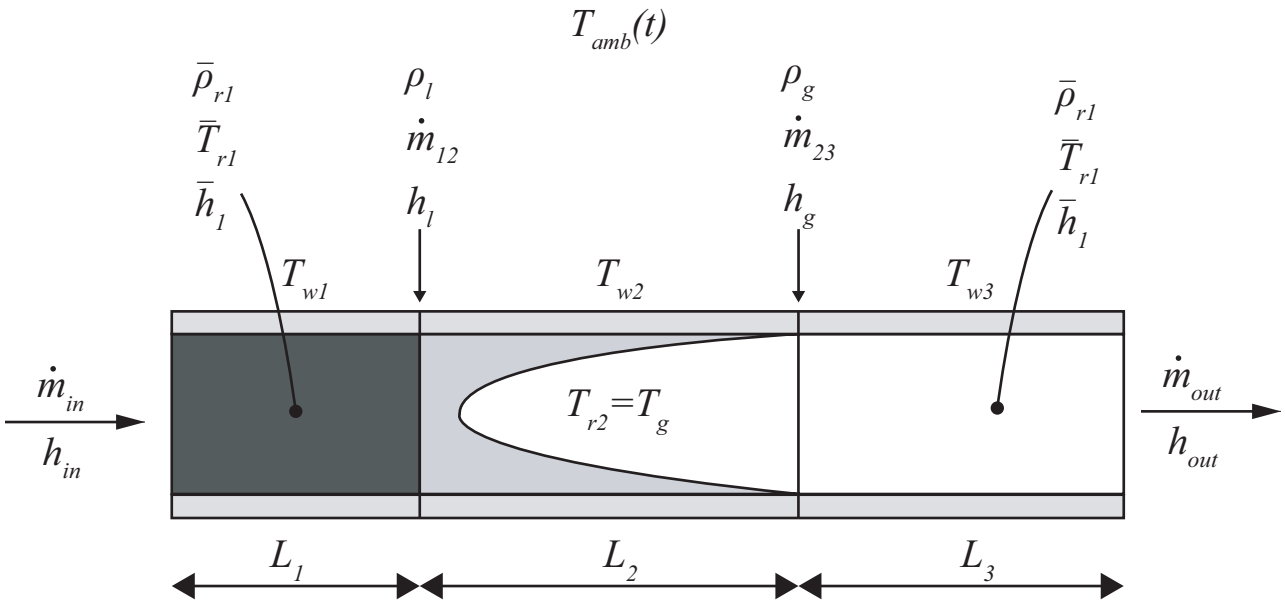

Figure 2.1: Schematic of a general MB-model

region is modeled as a control volume (CV) with variable boundaries using average properties including temperature, enthalpy and density. The governing equations of MB-model are one-dimensional mass balance (2.1),

$$\frac{\partial A\rho}{\partial t} + \frac{\partial \dot{m}}{\partial z} = 0 \tag{2.1}$$

and one-dimensional energy balance neglecting the axial conduction, radiation and the viscous stresses (2.2),

$$\frac{\partial A\rho h - Ap}{\partial t} + \frac{\partial \dot{m}h}{\partial z} = \pi D\alpha(T_w T_r) \tag{2.2}$$

Also, a simplified differential energy balance for the wall of the heat exchanger is derived by substitution of all flow terms in (2.2) for zero resulted in (2.3),

$$C_w\rho_w A_w \frac{\partial T_w}{\partial t} = \alpha_i \pi D_i(T_w f - T_w) + \alpha_o \pi D_o(T_{amb} - T_w) \tag{2.3}$$

According to the MB-model idea, the equations (2.1),(2.2),(2.3) are integrated over the three regions. Moreover, for the integrations, Leibniz's integral rule explained in Appendix A is applied over each region.

- **Superheated region**

  If the heat exchanger is considered as a condenser, the working fluid entering the condenser is in the superheated phase so that the first region, L_1, indicates the superheated region. Equation (2.4) shows the integration of the governing mass balance over the first region,

$$\int_0^{L_1} \frac{\partial A\rho}{\partial t}\, dz + \int_0^{L_1} \frac{\partial \dot{m}}{\partial z}\, dz = 0 \tag{2.4}$$

  Applying Leibniz's integral rule on (2.4) gives,

$$A\frac{d}{dt}\int_0^{L_1} \rho\, dz - A\rho L_1 \frac{dL_1}{dt} + \dot{m}_{12} - \dot{m}_{in} = 0 \tag{2.5}$$

  Note that the density at the interface between region 1 and 2 is equal to the saturated vapor density, ρ_g, that is,

$$\rho\, L_1 = \rho_g \tag{2.6}$$

  Furthermore, pressure, p, and mean enthalpy, $\bar{h}$, define the state of the superheated region where,

$$\bar{h}_1 = \frac{1}{2}(h_{in} + h_g) \tag{2.7}$$

  where the inlet enthalpy, h_{in}, is determined from the boundary conditions, and saturated enthalpy, h_g, is only a function of the pressure. Also, the first term can be approximated by mean density multiplied by length of the region as below,

$$\int_0^{L_1} \rho\, dz \approx L_1\, \bar{\rho}_1 \tag{2.8}$$

  In general, all required dependent variables such as the mean density, $\bar{\rho}_1$, and mean temperature, $\bar{T}_1$, are a function of the pressure and the region mean enthalpy, that is,

$$\bar{\rho}_1 \approx f(p, \bar{h}_1) \tag{2.9}$$

$$\bar{T}_1 \approx f(p, \bar{h}_1) \tag{2.10}$$

  Eventually, substitution of (2.6) and (2.8) into (2.5) for the superheated region gives

$$A\left[L_1 \frac{d\bar{\rho}_1}{dt} + (\bar{\rho}_1 - \rho_g)\frac{dL_1}{dt}\right] = \dot{m}_{in} - \dot{m}_{12} \tag{2.11}$$

Given that pressure, mean enthalpy and length of the section are the state variables in each region, all other dependent variables should be represented by the state variables. (2.11) using chain rule reads,

$$\frac{d\bar{\rho}_1}{dt} = \left.\frac{\partial\bar{\rho}_1}{dp}\right|_h \frac{dp}{dt} + \left.\frac{\partial\bar{\rho}_1}{d\bar{h}_1}\right|_p \frac{d\bar{h}_1}{dt} \tag{2.12}$$

then substitution of (2.7) into (2.12) results in,

$$\frac{d\bar{\rho}_1}{dt} = \left(\left.\frac{\partial\bar{\rho}_1}{dp}\right|_h + \frac{1}{2}\left.\frac{\partial\bar{\rho}_1}{d\bar{h}_1}\right|_p\right)\frac{dp}{dt} + \frac{1}{2}\left.\frac{\partial\bar{\rho}_1}{d\bar{h}_1}\right|_p \frac{dh_{in}}{dt} \tag{2.13}$$

where $\frac{dh_{in}}{dt}$ is a boundary condition of the heat exchanger and considered zero in this work because the changes of enthalpy in the boundary is negligible. Then, (2.13) is inserted into mass balance equation (2.11) such that the final mass balance equation for the superheated region becomes,

$$A\left[L_1\left(\left.\frac{\partial\bar{\rho}_1}{dp}\right|_h + \frac{1}{2}\left.\frac{\partial\bar{\rho}_1}{d\bar{h}_1}\right|_p\right)\frac{dp}{dt} + \frac{1}{2}L_1\left.\frac{\partial\bar{\rho}_1}{d\bar{h}_1}\right|_p \frac{dh_{in}}{dt} + (\bar{\rho}_1 - \rho_g)\frac{dL_1}{dt}\right] = \dot{m}_{in} - \dot{m}_{12} \tag{2.14}$$

Then, the same integration process is conducted over the energy balance equation (2.2) to transfer the equation into time derivative of the state variables. In this regards, integration of (2.2) over the superheated region reads,

$$\int_0^{L_1} \frac{\partial A\rho h - Ap}{\partial t}\,dz + \int_0^{L_1} \frac{\partial \dot{m}h}{\partial z}\,dz = \int_0^{L_1} \pi D\alpha_i(T_w T_r)\,dz \tag{2.15}$$

Again applying Leibniz integral rule on the first term and integrating the other terms by assuming constant heat transfer coefficient results in,

$$A\frac{d}{dt}\int_0^{L_1} \rho h\,dz - A(\rho L_1)(hL_1)\frac{dL_1}{dt} - AL_1\frac{dp}{dt} + \dot{m}_{12}h_1 - \dot{m}_{in}h_{in} = \pi D_i\alpha_{i1}L_1(T_{w1} - \bar{T}_{wf1}) \tag{2.16}$$

where the first integral can be evaluated as,

$$\int_0^{L_1} \rho h\,dz = L_1\bar{\rho}_1\bar{h}_1 \tag{2.17}$$

, and the second term can be written as follows,

$$\rho L_1 = \rho_g \quad , \quad hL_1 = h_g \tag{2.18}$$

Thus, inserting (2.18) into (2.16) gives,

$$A\frac{d(L_1\bar{\rho}_1\bar{h}_1)}{dt} - A\rho_g h_g\frac{dL_1}{dt} - AL_1\frac{dp}{dt} + \dot{m}_{12}h_1 - \dot{m}_{in}h_{in} = \pi D_i\alpha_{i1}L_1(T_{w1} - \bar{T}_{wf1}) \tag{2.19}$$

substitution of (2.7) and rearranging (2.19) reads,

$$\begin{aligned}
&A\left(\frac{1}{2}\bar{\rho}_1(h_{in}+h_g) - \rho_g h_g\right)\frac{dL_1}{dt} \\
&+\frac{1}{2}AL_1\left(\bar{\rho}_1 + \frac{1}{2}(h_{in}+h_g)\left.\frac{\partial\bar{\rho}_1}{d\bar{h}_1}\right|_p\right)\frac{dh_{in}}{dt} \\
&+\frac{1}{2}AL_1\left[\bar{\rho}_1\frac{dh_g}{dp} + (h_{in}+h_g)\left(\left.\frac{\partial\bar{\rho}_1}{dp}\right|_h + \frac{1}{2}\left.\frac{\partial\bar{\rho}_1}{d\bar{h}_1}\right|_p\frac{dh_g}{dp}\right)\right]\frac{dp}{dt} \\
&-AL_1\frac{dp}{dt} + \dot{m}_{12}h_1 - \dot{m}_{in}h_{in} \\
&= \pi D_i\alpha_{i1}L_1(T_{w1} - \bar{T}_{wf1})
\end{aligned} \tag{2.20}$$

rewriting (2.20) results in the final energy balance equation for the superheated region as follows,

$$\begin{aligned}
&\frac{1}{2}A\left[[\bar{\rho}_1(h_{in}+h_g) - 2\rho_g h_g]\frac{dL_1}{dt}\right. \\
&+\left(L_1\bar{\rho}_1 + \left.\frac{\partial\bar{\rho}_1}{dh}\right|_p\right)\frac{dh_{in}}{dt} \\
&\left.+L_1\left[\bar{\rho}_1\frac{dh_g}{dp} + (h_{in}+h_g)\left(\left.\frac{\partial\bar{\rho}_1}{dp}\right|_h + \frac{1}{2}\left.\frac{\partial\bar{\rho}_1}{d\bar{h}_1}\right|_p\frac{dh_g}{dp} - 2\right)\right]\frac{dp}{dt}\right] \\
&= \dot{m}_{in}h_{in} - \dot{m}_{12}h_1 + \pi D_i\alpha_{i1}L_1(T_{w1} - \bar{T}_{wf1})
\end{aligned} \tag{2.21}$$

Also, the energy balance in the wall of the superheated region can be formulated as below,

$$C_w\rho_w A_w\frac{dT_{w1}}{dt} = 2\pi r_i\,\alpha_{i1}(\bar{T}_1 - T_{w1}) + 2\pi\, r_o\,\alpha_o(T_a - T_{w1}). \tag{2.22}$$

Ultimately, the mass balance and energy balance, (2.21) and (2.14), are all formatted based on time derivatives of the state variables and the boundary condition representing the dynamic of

the superheated region, and (2.22) accounts for the dynamic of the wall temperature in this region.

- **Two-phase region**

  In two-phase region, the procedure is based on the same idea as the superheated region where the mass balance and the energy balance are integrated over the two-phase region. Conversely, the difference in this region is the way that the independent variables are calculated since the mean variable method does not work in the the two-phase region. In this region, the average density is calculated using average liquid fraction which is defined as follows,

$$\bar{\eta} = \frac{1}{L_2}\int_{L_1}^{L_1+L_2} \eta \, dz \tag{2.23}$$

where $\eta = \frac{A_l}{A_t p}$ and $\bar{\eta}$ is only a function of the pressure and calculated by Ziki correlation defined as below,

$$\bar{\eta} = 1 - \frac{1-\mu^{2/3}\left(1-ln\left(\mu^{2/3}\right)\right)}{\left(1-\mu^{2/3}\right)^2} \tag{2.24}$$

where, μ is density ratio defined as,

$$\mu = \frac{\rho_g}{\rho_l} \tag{2.25}$$

The flow in the two-phase region is assumed homogeneous at equilibrium conditions such that the mean density is,

$$\bar{\rho}_2 = \bar{\eta}\rho_g + (1-\bar{\eta})\rho_l \tag{2.26}$$

Now, the integration of mass balance over the two-phase region (2.27) can be proceeded using the average liquid fraction method as follows,

$$\int_{L_1}^{L_1+L_2} \frac{\partial A\rho}{\partial t}\, dz + \int_{L_1}^{L_1+L_2} \frac{\partial \dot{m}}{\partial z}\, dz = 0 \tag{2.27}$$

Applying Leibniz integral rule leads to,

$$A\frac{d}{dt}\int_{L_1}^{L_1+L_2} \rho_2 \, dz + A\rho_l \frac{dL_1}{dt} - A\rho_g \frac{d(L_1+L_2)}{dt} = \dot{m}_{12} - \dot{m}_{23} \tag{2.28}$$

where,

$$\int_{L_1}^{L_1+L_2} \rho_2 \, dz \approx L_2 \bar{\rho}_2 \tag{2.29}$$

And, using chain rule and the average liquid (2.26), time derivative of $\bar{\rho}_2$ can be written as,

$$\frac{d\bar{\rho}_2}{dt} = \left(\bar{\eta} \frac{d\rho_l}{dp} + (1-\bar{\eta}) \frac{d\rho_g}{dp} \right) \frac{dp}{dt}. \tag{2.30}$$

Substitution of (2.29) into (2.28) and using (2.30) give the final mass balance equation for the two-phase region as below,

$$A_c L_2 \left(\bar{\eta} \frac{d\rho_g}{dP} + (1-\bar{\eta}) \frac{d\rho_l}{dP} \right) \frac{dP}{dt} + A_c (\rho_g - \rho_l) \frac{dL_1}{dt} + A_c \bar{\eta} (\rho_g - \rho_l) \frac{dL_2}{dt} = \dot{m}_{\text{int1}} - \dot{m}_{\text{int2}}. \tag{2.31}$$

Moreover, the integration of energy balance over the two-phase region represented as below,

$$\int_{L_1}^{L_1+L_2} \frac{\partial A\rho h - Ap}{\partial t} \, dz + \int_{L_1}^{L_1+L_2} \frac{\partial \dot{m} h}{\partial z} \, dz = \int_{L_1}^{L_1+L_2} \pi D \alpha_i (T_w T_r) \, dz, \tag{2.32}$$

can be formulated as below using Leibniz integral rule,

$$\begin{aligned} &A_c \frac{d}{dt} \int_{L_1}^{L_1+L_2} \rho_2 h_2 dz + A_c \rho_g h_g \frac{dL_1}{dt} - A_c L_1 \frac{dP_c}{dt} - A_c \rho_l h_l \frac{d(L_1+L_2)}{dt} - A_c L_2 \frac{dP_c}{dt} \\ &= \dot{m}_{\text{int1}} h_g - \dot{m}_{\text{int2}} h_l + 2\pi r_{i,c} L_2 \alpha_{i,2} (T_{w,2} - T_{\text{wf},2}). \end{aligned} \tag{2.33}$$

The integral term of (2.33) can be approximated by the following equation,

$$\frac{d}{dt} \int_{L_1}^{L_1+L_2} \rho_2 h_2 dz = \frac{d}{dt} \int_{L_1}^{L_1+L_2} \left(\bar{\eta} \rho_l h_l + (1-\bar{\eta}) \rho_g h_g \right) dz. \tag{2.34}$$

After taking the integral over left half side and using chain rule, it is reformulated as below,

$$\begin{aligned} \frac{d}{dt} \int_{L_1}^{L_1+L_2} \rho_2 h_2 dz &= L_2 \left[\bar{\eta} \frac{d(\rho_l h_l)}{dp} + (1-\bar{\eta}) \frac{d(\rho_g h_g)}{dp} \right] \frac{dp}{dt} \\ &+ \left\{ \bar{\eta} \rho_l h_l + (1-\bar{\eta}) \rho_l h_l \right\} \frac{dL_2}{dt}. \end{aligned} \tag{2.35}$$

Substitution of (2.35) into (2.33) gives the final energy balance equation for the two-phase region as below,

$$\begin{aligned} &A (\rho_g h_g - \rho_l h_l) \frac{dL_1}{dt} + A_c L_2 \left[\bar{\eta} \frac{d(\rho_g h_g)}{dp} + (1-\bar{\eta}) \frac{d(\rho_l h_l)}{dp} - 1 \right] \frac{dp}{dt} \\ &+ A \bar{\eta} (\rho_g h_g - \rho_l h_l) \frac{dL_2}{dt} = \dot{m}_{\text{int1}} h_g - \dot{m}_{\text{int2}} h_l + 2\pi r_{i,c} L_2 \alpha_{i,2} (T_{\text{wf},2} - T_{w,2}). \end{aligned} \tag{2.36}$$

Also, the energy balance for the wall of the two-phase region can be formulated as below,

$$C_w \rho_w A_w \frac{dT_{w,2}}{dt} = 2\pi\, r_i\, \alpha_{i2}(\bar{T}_2 - T_{w2}) + 2\pi\, r_o\, \alpha_o(T_a - T_{w2}). \tag{2.37}$$

Ultimately, the two governing equations over the two-phase region, (2.31) and (2.36), represents the dynamic model of this region, and (2.37) accounts for the dynamic of the wall temperature in this region.

- **Sub-cooled region**

The procedure is identical to superheated region for deriving the dynamic equations of the sub-cooled region. Therefore, for the sake of shortness, the final mass balance (2.38) and energy balance (2.39) dynamic equations are illustrated,

$$\begin{aligned} &A\,(\rho_l - \bar{\rho}_3)\,\frac{dL_1}{dt} + A\,(\rho_l - \bar{\rho}_3)\,\frac{dL_2}{dt} + \frac{1}{2}AL_3\frac{\partial \bar{\rho}_3}{\partial \bar{h}_3}\frac{dh_{out}}{dt} \\ &+ AL_3\left(\frac{1}{2}\frac{\partial \bar{\rho}_3}{\partial \bar{h}_3}\frac{\partial h_l}{\partial p} + \frac{\partial \bar{\rho}_3}{\partial p}\right)\frac{dp}{dt} = \dot{m}_{23} - \dot{m}_{out}. \end{aligned} \tag{2.38}$$

And,

$$\begin{aligned} &A\left(\frac{1}{2}L_3(h_l + h_{out})\left(\frac{1}{2}\frac{\partial \bar{\rho}_3}{\partial \bar{h}_3}\frac{\partial h_l}{\partial p} + \frac{\partial \bar{\rho}_3}{\partial p}\right) - 1\right)\frac{dp}{dt} + A\left(\rho_l h_l - \frac{1}{2}\bar{\rho}_3\,(h_l + h_{out})\right)\frac{dL_1}{dt} \\ &+ A\left(\rho_l h_l - \frac{1}{2}\bar{\rho}_3\,(h_l + h_{out})\right)\frac{dL_2}{dt} + A\left(\frac{1}{2}\bar{\rho}_3 L_3 + \frac{1}{4}L_3(h_l + h_{out})\frac{\partial \bar{\rho}_3}{\partial \bar{h}_3}\right)\frac{dh_{out}}{dt} \\ &= \dot{m}_{23}h_l - \dot{m}_{out}h_{out} + 2\pi r_i L_3 \alpha_{i,3}(T_{w,3} - \bar{T}_3). \end{aligned} \tag{2.39}$$

Also, the energy balance for the wall of the sub-cooled region reads,

$$C_w \rho_w A_w \frac{dT_{w3}}{dt} = 2\pi\, r_i\, \alpha_{i3}(\bar{T}_3 - T_{w3}) + 2\pi\, r_o\, \alpha_o(T_{amb} - T_{w3}) \tag{2.40}$$

Ultimately, the mass balance (2.38) and the energy balance (2.39) represents the dynamic of the sub-cooled region, and (2.40) is the dynamic of the wall temperature in this region.

To sum up, all 9 final mass and energy balance equations, (2.20), (2.21), (2.22), (2.31), (2.36), (2.37), (2.38), (2.39) and (2.40) make a system of 9 equations and 7 independent variables (state variables). The system state is denoted by the vector of $x(t)$,

$$x^T(t) = \begin{bmatrix} L_1(t) & L_2(t) & p(t) & h_{out}(t) & T_{w1}(t) & T_{w2}(t) & T_{w3}(t) \end{bmatrix}.$$

There are two dummy variables which are $\dot{m}_{12}$ and $\dot{m}_{23}$ that can be eliminated such that a 7^{th} order system of ordinary differential equations (ODEs) reveals the nonlinear dynamic model of a sub-critical heat exchanger. Eventually, the 7^th order system of MB-model ODEs can be illustrated as below,

$$\Theta(x)\dot{x}(t) = \Gamma(x,b) \tag{2.41}$$

where $\Theta(x)$ is a 7×7 matrix consisting of dependent variables, $D(x)$, where they are the function of the state variables, $x(t)$.

$$D(x) = \begin{Bmatrix} \bar{\rho}_1 & \bar{\rho}_2 & \bar{\rho}_3 & \frac{\partial \bar{\rho}_1}{dh}\Big|_p & \frac{\partial \bar{\rho}_1}{dp}\Big|_h & \frac{\partial \bar{\rho}_2}{dh}\Big|_p & \frac{\partial \bar{\rho}_2}{dp}\Big|_h & \frac{\partial \bar{\rho}_3}{dh}\Big|_p & \frac{\partial \bar{\rho}_3}{dp}\Big|_h \end{Bmatrix} \tag{2.42}$$

And, $\Gamma(x,b)$ is a 7×1 vector where it is a function of state variables, x, and boundary conditions,

$$b = \begin{Bmatrix} \dot{m}_{in} & \dot{m}_{out} & h_{in} & \dot{h}_{in} & T_{amb} \end{Bmatrix}. \tag{2.43}$$

Since (2.41) is a full rank system of equations, it can be formulated in standard format of first order ODEs as below,

$$\dot{x}(t) = \Theta^{-1}(x)\Gamma(x,b) \tag{2.44}$$

where (2.44) will be used as a control-oriented dynamic model of a heat exchanger.

Although the derived model has considered a heat exchanger as a condenser, this dynamic model is capable of being simply formulated for sub-critical evaporators as well.

2.1.2 Single Region Model

A single region model represents a simple rough dynamic model of a heat exchanger where it is an appropriate model for control purposes. This dynamic model can be utilized when the work-

ing fluid is single-phase or in Trans-critical conditions where there are not separate phase regions. Although this single region model has a potential for control purposes, it is not as accurate as the MB-model so that it puts the burden on control system design.

The single region dynamic model is derived based on mass balance and energy balance in working fluid region and also energy balance in the wall of the heat exchanger. A schematic of a single region model is illustrated in figure 2.2. To derive the dynamic equations, the mass balance

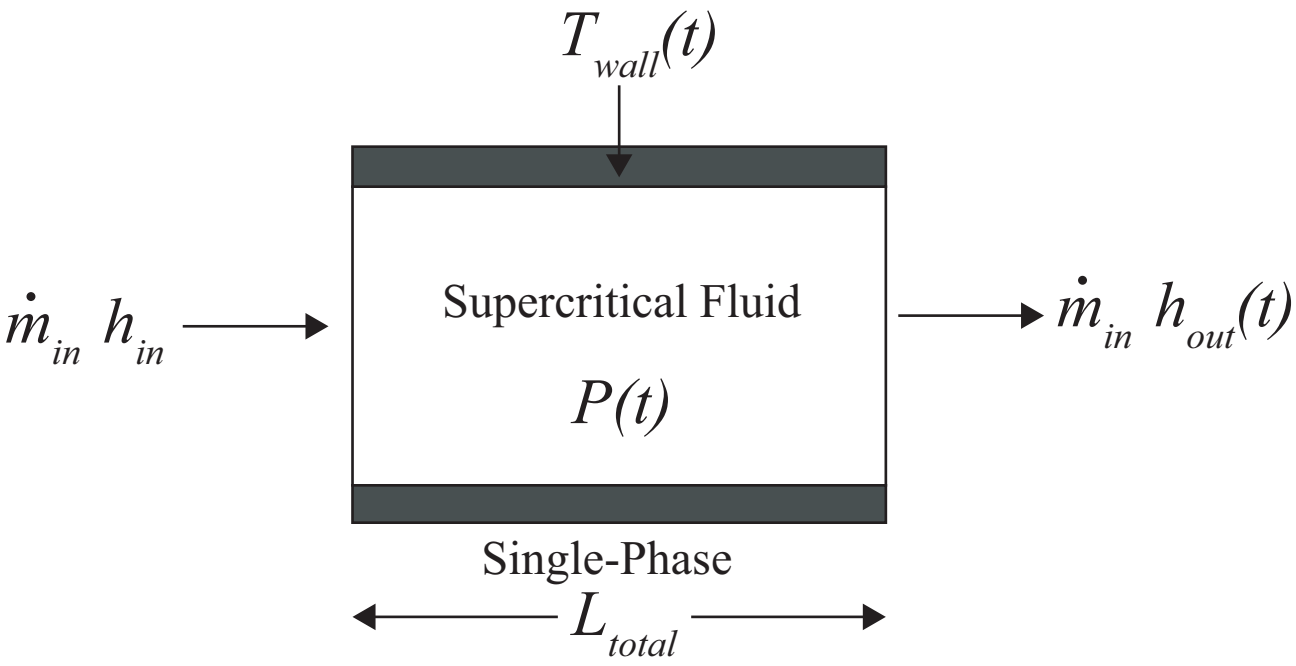

Figure 2.2: conceptual scheme of a single region model of a heat exchanger

(2.1) and energy balance (2.2) are recalled such that they are integrated over the tube length of the heat exchanger as below,

$$\int_0^L \frac{\partial A\rho}{\partial t}\,dz + \int_0^L \frac{\partial \dot{m}}{\partial z}\,dz = 0 \tag{2.45}$$

Applying Leibniz's integral rule on (2.45) gives,

$$A\frac{d}{dt}\int_0^L \rho\,dz - A\rho L\frac{dL}{dt} + \dot{m}_{out} - \dot{m}_{in} = 0 \tag{2.46}$$

According to the mean variable method explained in MB-model, the integral in (2.46) can be

formulated as follows,

$$AL\left(\left.\frac{\partial\bar{\rho}}{\partial p}\right|_h \frac{dp}{dt}+\frac{1}{2}\left.\frac{\partial\bar{\rho}}{\partial\bar{h}}\right|_p \frac{dh_{out}}{dt}\right)=\dot{m}_{in}-\dot{m}_{out} \tag{2.47}$$

where this is the final mass balance equation.

The integration process is carried out over energy balance PDE such that the PDE is transferred into an ODE. to derive the final energy balance equation for single region model. This ODE coupled with mass balance ODE capture the working fluid dynamics.

$$\int_0^L \frac{\partial A\rho h-Ap}{\partial t}\,dz+\int_0^L \frac{\partial\dot{m}h}{\partial z}\,dz=\int_0^L \pi D\alpha_i(T_wT_r)\,dz \tag{2.48}$$

The same procedure as MB-model is performed to derive the final energy balance equation in an ODE form so that using Leibniz integral rule and the mean variable method, (2.48) turns into the following equation,

$$AL\left[\left(\bar{h}\left.\frac{\partial\bar{\rho}}{\partial p}\right|_h-1\right)\frac{dp}{dt}+\frac{1}{2}\left(\left.\frac{\partial\bar{\rho}}{\partial\bar{h}}\right|_p\right)\frac{dh_{out}}{dt}\right]=\dot{m}_{in}h_{in}-\dot{m}_{out}h_{out}+\pi LD_i\alpha_i\,(T_w-\bar{T}). \tag{2.49}$$

where,

$$\bar{h}=\frac{1}{2}(h_{out}+h_{in}),$$

$$\bar{\rho}=f(p,\bar{h}),$$

$$\left.\frac{\partial\bar{\rho}}{\partial p}\right|_h=f(p,\bar{h}),$$

and

$$\left.\frac{\partial\bar{\rho}}{\partial h}\right|_p=f(p,\bar{h}),$$

Finally, to capture wall temperature dynamics, energy balance equation for the wall using mean variable method is formulated as a lumped parameters model as below,

$$C_w\rho_wA_w\frac{dT_w}{dt}=2\pi\,r_i\,\alpha_i(\bar{T}-T_w)+2\pi\,r_o\,\alpha_o(T_{amb}-T_w) \tag{2.50}$$

Ultimately, (2.47),(2.49) and (2.50) represent the single region dynamic model of a heat exchanger where state vector $x(t)$ is,

$$x^T(t) = \begin{bmatrix} p(t) & h(t) & T_w(t) \end{bmatrix}. \tag{2.51}$$

The final 3^{rd} order single region dynamic model can be represented as below,

$$\Theta(x)\dot{x}(t) = \Gamma(x,b) \tag{2.52}$$

where $\Theta(x)$ is a 3×3 matrix consisting of dependent variables, $D(x)$, where they are the function of the state variables, $x(t)$.

$$D(x) = \begin{Bmatrix} \bar{\rho} & \bar{h} & \frac{\partial\bar{\rho}}{dh}\Big|_p & \frac{\partial\bar{\rho}}{dp}\Big|_h \end{Bmatrix} \tag{2.53}$$

And, $\Gamma(x,b)$ is a 3×1 vector where it is a function of state variables, x, and boundary conditions, b,

$$b = \begin{Bmatrix} \dot{m}_{in} & \dot{m}_{out} & h_{in} & T_{amb} \end{Bmatrix}. \tag{2.54}$$

Since (2.52) is a full rank system of equations, it can be formulated in standard format, a system of first order ODEs, as below,

$$\dot{x}_{(}t) = \Theta^{-1}(x)\Gamma(x,b) \tag{2.55}$$

where (2.55) will be used as a control-oriented dynamic model of a heat exchanger.

2.1.3 Lumped Capacitance Model

Lumped capacitance model (LC-model) captures temperature dynamics of hot side, cold side and wall of the heat exchanger as state variables. This model can be utilized to model a counter flow recuperator or preheater in a thermal system where either side of the heat exchanger contain a single-phase flow as shown in figure 2.3. It is worth mentioning that in Trans-critical condition, this model will be used because the fluid is not in gas phase neither the liquid phase so that LC-model captures an approximate dynamic behavior of a recuperator.

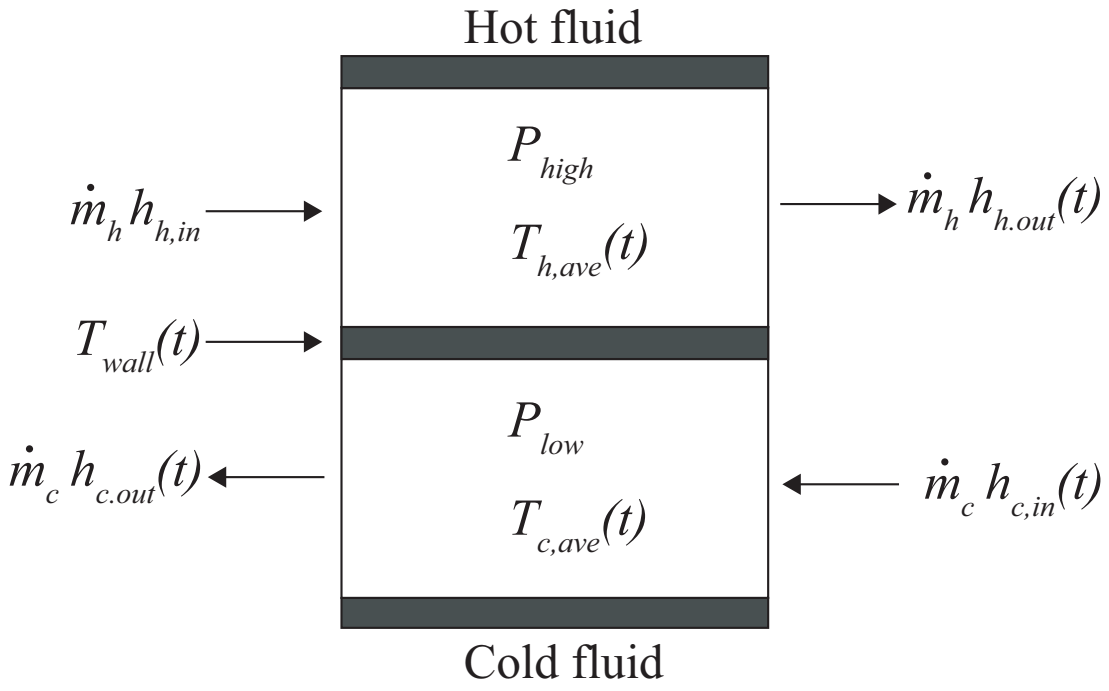

Figure 2.3: schematic scheme of an LC-model of a counter flow single-phase heat exchanger

In LC-model, energy balance ODEs for hot side, cold side and wall of the heat exchanger are formed using mean variable method such that they provide a 3^{rd} order dynamic model as follows,

$$\frac{T_{h,out}}{dt} = \left(\frac{2}{\bar{\rho}_h C_h A_h L}\right)\left[\dot{m}_{in} C_h (T_{h,in} - T_{h,out}) + \pi L \alpha_h D_h (T_w - \bar{T}_h)\right], \tag{2.56}$$

$$\frac{T_{c,out}}{dt} = \left(\frac{2}{\bar{\rho}_c C_c A_c L}\right)\left[\dot{m}_{in} C_c (T_{c,in} - T_{c,out}) + \pi L \alpha_c D_c (T_w - \bar{T}_c)\right], \tag{2.57}$$

$$\frac{T_w}{dt} = \left(\frac{\pi}{\rho_w C_w A_w}\right)\left[D_c \alpha_c (\bar{T}_c - T_w) - D_h \alpha_h (T_w - \bar{T}_h)\right], \tag{2.58}$$

where,

$$\bar{T}_h = \frac{1}{2}(T_{h,out} + T_{h,in}),$$

and,

$$\bar{T}_c = \frac{1}{2}(T_{c,out} + T_{c,in}).$$

Also uniform working fluid pressure is assumed for each side of the heat exchanger. The state vector $x(t)$ is,

$$x^T(t) = \begin{bmatrix} T_{h,out} & T_{c,out} & T_w \end{bmatrix}.$$

Also, boundary conditions contain,

$$b = \left\{ \dot{m}_{in} \quad \dot{m}_{out} \quad T_{in} \quad p_h \quad p_c \right\}.$$

Therefore, the dependent variables can be calculated using thermodynamic state equations as follows,

$$\bar{\rho}_h = f(p_h, \bar{T}_h), \qquad \bar{\rho}_c = f(p_c, \bar{T}_c)$$

Ultimately, (2.56), (2.57) and (2.58) form a 3^{rd} order LC-model (2.59) of a heat exchanger where it contains two single-phase counter-cross flows exchanging heat with each other represented as follows.

$$\dot{x}(t) = \Theta^{-1}(x)\Gamma(x,b) \tag{2.59}$$

2.1.4 Heat Transfer Coefficient Correlation

Heat transfer coefficient correlation is an algebraic empirical equation. There are a variety of empirical correlations to calculate the heat transfer coefficient for single-phase, two-phase or Trans-critical conditions. A comprehensive survey is found in [36] where the accuracy of various correlations were investigated. In this work, the single-phase heat transfer coefficient is calculated by Gnielinski's correlation referred in [29] as below,

$$Nu = \frac{Pr(\zeta/8)(Re - 1000)}{1 + 12.7(\zeta/8)^{1/2}(Pr^{2/3} - 1)} \tag{2.60}$$

where Re and Pr are the Reynold number and Prandtl number respectively, and ζ is the Moody friction factor for smooth pipes such that it can be computed using Petukhov's correlation [29] as follows,

$$\zeta = (0.790\,ln(Re) - 1.64)^{-2}. \tag{2.61}$$

And, this equation is valid for $3000 < Re < 5.10^6$ and $0.5 < Pr < 2000$ assuming uniform heat flux and temperature. The Nusselt, Reynold and Prandtl numbers are determined by,

$$Nu = \frac{\alpha D}{\lambda}, \quad Pr = \frac{\eta c_p}{\lambda}, \quad Re = \frac{\dot{m} D}{A\eta}, \tag{2.62}$$

where λ, η And c_p denote the thermal conductivity, the dynamic viscosity, the specific isobaric heat capacity respectively. Also, A is the tube cross-sectional area. Eventually, using (2.60),(2.61) and (2.62), the heat transfer coefficient, α, of a single flow in a horizontal tube is derived.

Furthermore, the heat transfer coefficient of a two-phase flow, α_{tp}, for the convective heat transfer in a horizontal tube can be computed using the single-phase heat transfer coefficient of liquid phase, α_l, and gas phase, α_g, using a correlation referred by [23] as below,

$$\alpha_{tp} = \alpha_l \left[\left[(1-x) + 1.2x^{0.4}(1-x)(\frac{\rho_l}{\rho_g})^{0.37} \right]^{-2.2} + \left[\frac{\alpha_g}{\alpha_l} x^{0.01} \left(1 + 8(1-x)^{0.7}(\frac{\rho_l}{\rho_g})^{0.67} \right) \right]^{-2} \right]^{-0.5} \tag{2.63}$$

where x is the two-phase flow quality. α_l and α_g are the saturated liquid density and saturated gas density respectively.

Ultimately, it is noted that the heat transfer coefficient of the working fluid is a function of its mass flow rate, average temperature and pressure. As it was mentioned in MB-model, the heat transfer coefficient is constant in each phase region. Furthermore, Gnielinski's correlation for heat transfer coefficient calculation is valid for Trans-critical conditions.

2.2 Turbine Expander Static Model

In a thermal system consist of heat exchangers and expander, the expander dynamic is relatively negligible in comparison with the heat exchangers so that there is no need of a dynamic model for the expander. This section focuses on deriving a static model for a volumetric expander, scroll expander shown in figure 2.4. The volumetric expanders come with an internal built-in volume

ratio ($r_{v,in}$) corresponding to the ratio between inlet and outlet pocket volume.

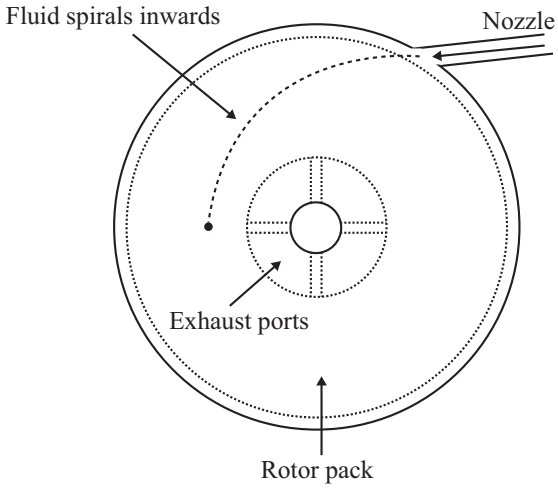

Figure 2.4: scroll turbine expander schematic

There are two physical phenomena occur in an expander, under-expansion and over-expansion, where the expander pressure ratio is not equal to the thermal system pressure ratio. Under-expansion happens when expander pressure ratio is lower than the system pressure ratio whereas over-expansion occurs under an opposite condition, which results in some loss rather than isentropic expansion. A semi-empirical thermodynamic model can is suitable such that a generic non-dimensional efficiency is defined according to a set of empirical data. In this regards, if ambient heat losses are neglected, a scroll expander can be modeled with isentropic effectiveness and filling factor where the isentropic effectiveness is defined as below,

$$\varepsilon = \frac{\dot{W}_{sh}}{\dot{m}(h_{in} - h_{out,s})}, \tag{2.64}$$

and the filling factor is defined by,

$$\phi = \frac{\dot{m}\, v_{in}}{\dot{V}_s} \tag{2.65}$$

where v_{in} is the specific volume of the inlet flow, the $\dot{V}_s$ is the theoretical swept volume flow rate of the expander and it quantifies the volumetric performance of the expander.

The isentropic effectiveness and the filling factor of the scroll expander are calculated using the empirical data. The isentropic effectiveness enables formulating the outlet enthalpy of the scroll expander as follows,

$$h_{out} = h_{in} - \varepsilon(h_{in} - h_{out,s}) \tag{2.66}$$

where $h_{out,s}$ is the expander isentropic outlet enthalpy which is calculated by

$$h_{out,s} = f(p_{out}, s_{in})$$

where $s_{in} = f(p_{in}, h_{in})$.

Furthermore, the filling factor defined by (2.65) enables calculating the expander internal mass flow rate such that the empirical data leads to estimating the filling factor where it is the function of the rotating speed, N, and the inlet density, ρ_{in}. Thus, according to the filling factor definition, the expander mass flow rate is,

$$\dot{m} = \frac{\dot{V}_{in}}{v_{in}} \tag{2.67}$$

where, the expander volume flow rate,$\dot{V}_{in}$ is defined as the product of the swept volume, V_s and the expander rotational speed (in RPS unit). Note that expander rotational speed is in RPM unit so that it must be divided by 60 to convert the unit such that,

$$\dot{m} = \phi \frac{V_s}{v_{in}} \frac{N}{60} \tag{2.68}$$

Ultimately, equations (2.66) and (2.68) will be used as a static model of a scroll expander for the final ORC model such that the expander outlet enthalpy defines the inlet enthalpy boundary condition, h_{in} of the recuperator at hot side, and the expander mass flow rate defines the recuperator inlet mass flow rate at hot side while defining the boundary condition of the evaporator outlet mass flow rate, $\dot{m}_out$. Moreover, the expander rotation speed, N, will be one of the control inputs to the control system where the expander load is achieved through coupling of the turbine expander to an asynchronous motor used as a generator. Hence, the expander rotational speed can be adjusted

by a regenerative Variable Frequency Drive (VFD). From the practical viewpoint, extensive power electronics are utilized to synchronize the generator phase with a power grid where the load system is connected.

2.3 Pump Static Model

This section provides a semi-empirical static model for a positive-displacement pump where such pump is characterized by its built-in maximum flow rate, $\dot{V}_{max,pp}$, and its global isentropic effectiveness, η_{pp}. This model expresses the internal reversibility of the pumping process along with the electromechanical losses of the electric motor as a lumped model. Similarly, this model is based on the same idea as the expander in the previous section.

In this model, the mass flow rate displaced by the pump is calculated as a function of the capacity fraction, X_{pp}, which is defined as the ratio between actual volume flow rate and maximum volume flow rate of the pump. The capacity fraction is adjusted in proportion to the rotation speed of the pump where a Variable Frequency Drive (VFD) adjusts the pump motor rotation speed. Thus the pump mass flow rate is calculated by,

$$\dot{m} = \frac{X_{pp}\dot{V}_{max,pp}}{v_{in}}, \tag{2.69}$$

where v_{in} is the specific volume of the inlet fluid and $\dot{V}_{max,pp}$ is the maximum volume flow rate of the pump.

Furthermore, if the fluid is assumed incompressible in the pump, the enthalpy of the outlet flow is determined using the global isentropic effectiveness, η_{pp}, by a semi-empirical formula as follows

,

$$h_{out} = h_{in} + \frac{P_{out} - P_{in}}{\eta_{pp}\,\rho_{in}} \tag{2.70}$$

where h_{in}, P_{in} and P_{out} are the boundary conditions, and ρ_{in} can be calculated using the thermodynamic state equation of the working fluid, that is $\rho_{in} = f(P_{in}, h_{in})$.

2.4 Organic Rankine Cycle Dynamic Model

This section frames two global model of an ORC system which are Sub-critical Organic Rankine Cycle (SORC) and Trans-critical Organic Rankine Cycle (TORC). The global models are built by interconnecting the model of the components developed in previous sections. Due to cyclic feature of ORC systems, output variables of each element determine the boundary conditions of the surrounding components. Figure 2.5 illustrates the interconnection of the ORC components in general. Moreover, heat source temperature and ambient temperature determine the boundary conditions of the global system where these variables act as the source of disturbance into the ORC system. Also, the control inputs are the pump rotation speed, the turbine expander rotation speed, and the condenser fan rotation speed.

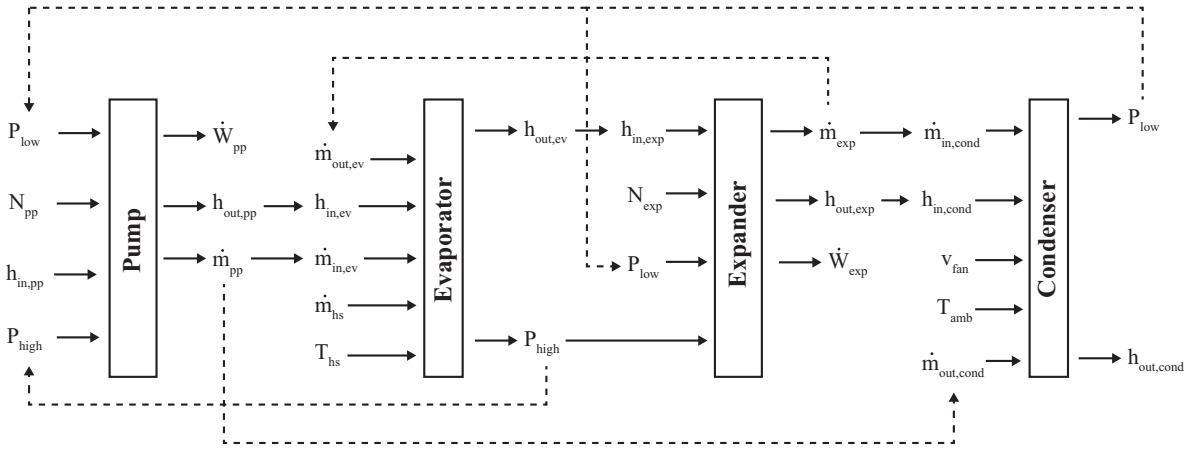

Figure 2.5: ORC global model illustrating the relations among the system components

2.4.1 Sub-critical Organic Rankine Cycle

Sub-critical Organic Rankine Cycle (SORC) is a type of ORC systems where the system operating conditions are in the sub-critical thermodynamic region shown in the T-s diagram of a sub-critical ORC system in figure 2.7.

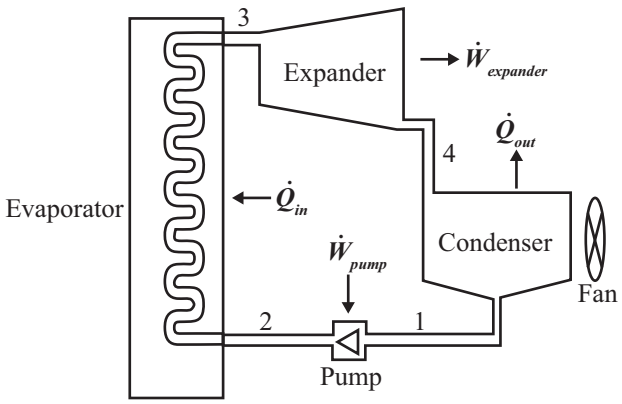

Figure 2.6: SORC system conceptual scheme

The net power produced by this SORC system is the area surrounded by points 1, 2, 3, 4, 9 and 1. In SORC systems, there are two sub-critical heat exchangers which are evaporator and condenser such that the MB-model built in section 2.1.1 are utilized where they make the system dynamic model whereas the static models of pump and turbine expander connects the heat exchangers as shown in figure 2.6.

Therefore, a control-oriented model of an SORC system consist of two sets of 7^th order sub-systems where they build a 14^th order system which is capable of describing the dominant behavior of the SORC system and is an appropriate choice for control purposes.

2.4.2 Trans-critical Organic Rankine Cycle

Super-critical or Trans-critical Organic Rankine Cycle (TORC) is another type of ORC system which is our primary focus in this work. The parameters of this TORC system is based on an ORC system located at North Alberta, Canada. Each component model of the TORC components is validated according to the literature stated in chapter 1.

Figure 2.7 compares T-s diagram of an SORC with a TORC. Similarly, a qualitative description of the TORC system is based on the interconnection of each component modeled in previous sections.

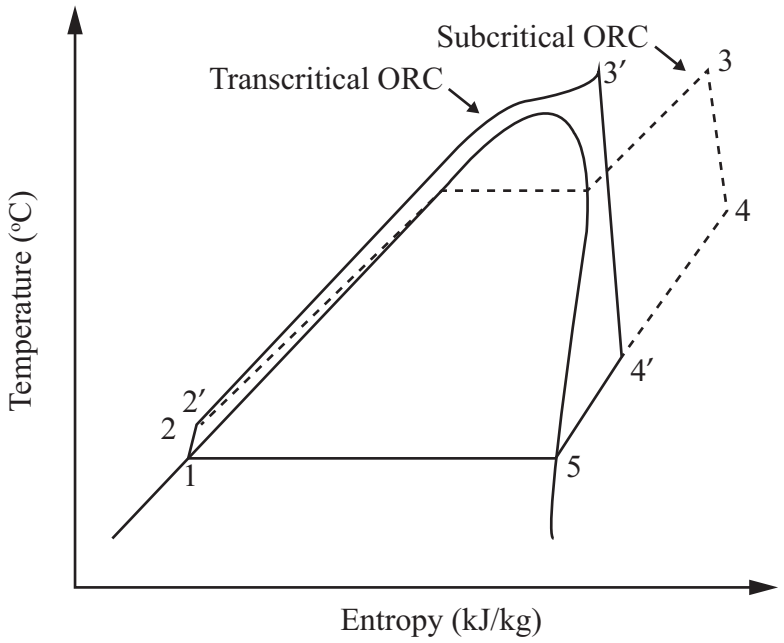

Figure 2.7: T-s diagram of Trans-critical versus Sub-critical ORC

Figure 2.8 illustrates a conceptual scheme of the TORC system which consists of three heat exchangers, evaporator, condenser, and recuperator. The recuperator is utilized to increase the cycle efficiency, and the working fluid is R134a which stands out among isentropic fluids.

In this TORC system, the evaporator is in contact with a secondary thermodynamic cycle and the secondary cycle is in direct touch with a heat source. The heat source is the waste heat of chimneys of a thermal power plant ran by fossil fuel so that using ORC system leads to regeneration of more power to the power grid. Since the ORC system is a regenerative power system, the power demand is alway assumed maximum value so that the control objective is to maintain the maximum efficiency of the system.

Since the evaporator and cold side of the recuperator work in trans-critical conditions where the fluid is not gas neither liquid so that the single region model elaborated in section 2.1.2 must be used as the dynamic model of the evaporator (2.55), and the lumped capacitance model developed in section 2.1.3 must be utilized as the dynamic model of the recuperator (2.59). Furthermore,

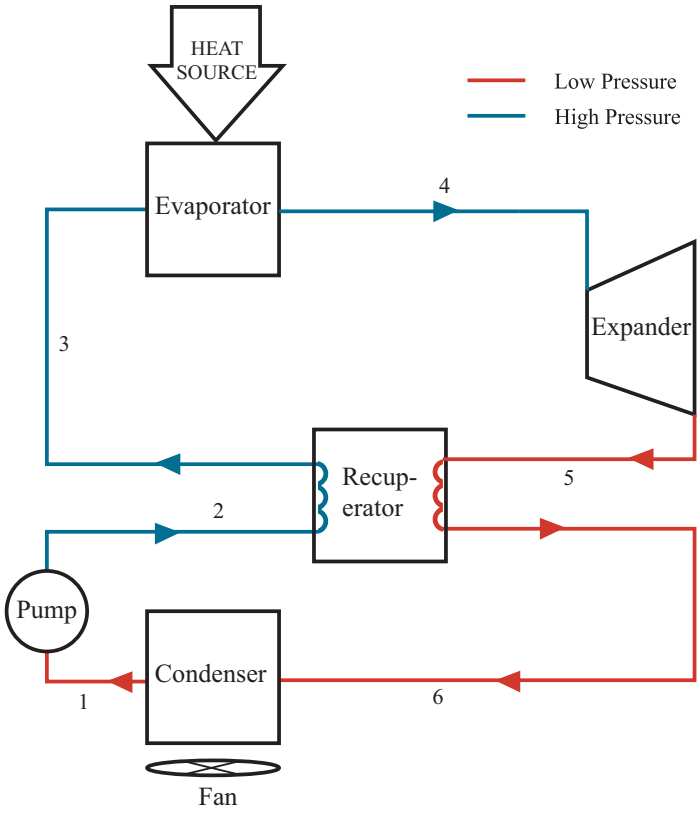

Figure 2.8: qualitative description of the TORC system in this work

similar to the SORC model, MB-model developed in section 2.1.1 is used as the dynamic model of the condenser (2.44). Finally, the static model of pump and turbine expander elaborated in section 2.2 and 2.3 respectively complete the final model of the TORC system. Also, the control inputs are the pump rotation speed, turbine expander rotation speed and condenser fan rotation speed, similar to the SORC system control inputs. Eventually, integration of the dynamic models of the heat exchangers and the static models of the pump and turbine expander provide the nonlinear model of TORC as follows,

$$\dot{x}(t) = \Theta^{-1}(x)\Gamma(x,b) \tag{2.71}$$

where $x(t)$ contains 13 state variables of TORC system, and b denotes boundary conditions which consist of control inputs and external inputs to the TORC system. Variation of external inputs such as fluctuation of heat source temperature is the source of disturbances into the system.

The source of disturbances is the fluctuation of heat source and the fluctuation of ambient temperature. In this work, the variation of ambient temperature is neglected as it does not have a considerable effect on performance. The fluctuation of heat source is considered as the main source of external disturbance where the heat source is a secondary thermal cycle. The secondary cycle works with Therminol 55 as its working fluid where Therminol 55 is a heat transfer fluid designed to provide consistent cost-effective heat transfer performance over a long life.

Ultimately, given that each component model is validated according to previous research works, the final TORC model simulations show the same behavior as physical behavior of TORC plants. For instance, a step change in pump rotation speed results in increasing the high pressure or a step change in expander results in decreasing the high pressure. This provides qualitative open loop characteristics of TORC nonlinear model.

Chapter 3

CONTROL DESIGN: ADAPTIVE OPTIMAL LYAPUNOV CONTROL USING CMAC NEURAL NETWORKS

This chapter elaborates on control system design for TORC systems. The control system is designed such that it addresses the control-oriented challenges stated in chapter 1. Recalling such challenges, set-point tracking, and disturbance rejection are the primary control design objectives. This enables the system to track the optimal operating conditions so that it maximizes system efficiency. First, this chapter explains a method for an optimal hyperplane design in state space where the optimal hyperplane is a state trajectory. Then, section 2 introduces CMAC as a type of neural networks and discusses the pros and cons of CMAC. Also, this section looks into the methodology of CMAC control system design so that it leads to making use of this controller as an adaptive system. Then, section 3 is about Kalman filter design where it is utilized as a state estimator for final control system design. Eventually, section 4 combines all sections to develop the final Adaptive Variable Structure Controller (AVSC). Ultimately, section 5 analyzes the stability of the designed control system using Lyapunov stability theory.

3.1 Optimal Hyperplane Design in State Space

In control design, an optimal hyperplane (H) in system state space will be designed such that the state of the system can have a sliding motion over this hyperplane. This control strategy is in class of Variable Structure Control (VSC) where this control class provides an effective and robust means of controlling nonlinear plants with uncertainties and disturbances [37]. The idea of VSC is to drive the nonlinear plant's state trajectory onto a designed sub-space of the state space where the sub-space is referred as a hyperplane in the state space. Thus, the plant dynamics are restricted

to this hyperplane so that this represents the closed-loop behavior of the plant. In VSC, the control can changes its structure which means the control is allowed to switch from one member to another member of a set of control structure. Hence, this ability enables the control system to combine useful properties of each structure although this introduces additional complexity. Moreover, VSC can reveal new features not presented in any of the structures. For instance, neither of structures may be asymptotically stable, but the system can be asymptotically stable [38]. In the well-known sliding mode control (SMC) which is in the VSC class, this hyperplane is called switching surface because if the state trajectory is above the surface, the control has one gain, while if the state trajectory is below the surface, the control switches to a different gain.

In 1977, Utkin [38] proposed a method for the VSC class called "method of equivalent control" to find ideal sliding motion condition ($S = Hx(t) = 0$). In this method, a time derivative of the hyperplane along the system state trajectory is set to zero where the resulting algebraic system is solved for the control. Eventually, the resulting control called equivalent control, $u_{eq}(t)$, is substituted into the original system. Once the equivalent control problem is solved where the control is a linear feedback control, K_{eq}, the attention must be concentrated on reachability problem. This problem is to select a state feedback control function, $\zeta(t)$, denoted as *robust term* which drives the state into the designed hyperplane or sub-space and thereafter maintain it within this sub-space. The function, $\zeta(t)$, is essentially a nonlinear function incorporating the discontinuous elements of the control law such that the final control law consists of the linear state feedback, $u_{eq}(t)$, and the nonlinear state feedback, $\zeta(t)$.

$$u(t) = u_{eq}(t) + \zeta(t), \qquad x(t) \in \Re^n$$

From practical viewpoint, to drive the state trajectory onto the hyperplane, the state perpetually passes backward and forward through a sliding manifold so that the control switches between

different values repeatedly. This undesirable phenomenon causing physical damage in actuators is known as *Chattering*. A simple and practical way of overcoming this issue is to soften the action of the nonlinear function, $\zeta(t)$ which is called *smoothing* control [39] although there are other proposed solutions for eliminating Chattering problem. For instance, Pieper 1998 [40] proposed a modified sliding function such that it effectively eliminated Chattering problem in sliding mode control.

As it was mentioned, designing the sliding hyperplane is of high importance as it shapes the system state trajectory or the dynamics behavior of the controlled system. Therefore, the other problem is to design this hyperplane. Therefore, a hyperplane design method can be carried out by quadratic minimization of a cost function proposed by Utkin [41]. Similarly, Pieper and Surgenor 1992 [42] developed this approach to design a discrete time sliding mode control. Then the designed controller was applied on a pulse-width modulated gantry crane system, and showed the effectiveness of this method. This method is conducted through a sequential process such that a cost function of the system state called cheap cost function (J_1) is defined as below,

$$J_1 = \frac{1}{2}\int_0^\infty x^T Q x\, dt \tag{3.1}$$

Solving this Linear Quadratic (LQ) optimization problem provides a initial value for the linear feedback control (u_{eq}) so that another LQ optimization problem with the actual cost function, J_2, can be solved by substitution of the initial control [39].

$$J_2 = \frac{1}{2}\int_0^\infty x^T Q x + u_{eq}^T R u_{eq}\, dt \tag{3.2}$$

Solving this LQ problem gives the optimal hyperplane in the state space, which leads to calculating the final linear state feedback gain, K_{eq}. Eventually, The linear state feedback, $u_{eq}(t)$ plus the nonlinear robust term, $\zeta(t)$, constructs the optimal sliding mode control law.

3.1.1 Control Structure

According to chapter 2, the nonlinear dynamic model of the system was developed and then linearized in a state space form as below.

$$\dot{x}(t) = Ax(t) + Bu(t) \tag{3.3}$$

where x $\in \Re^n$ u $\in \Re^m$ are the state and control vectors respectively. It is assumed that n>m and control input matrix, B, is full rank. First, controllability of the system is analyzed according to linear control systems theory. In this regards, controllability Gramian is constructed to determine whether the system is controllable. It is worth mentioning that controllability Gramian approach has an advantageous rather than the controllability matrix analysis approach because estimating the rank of the controllability matrix is ill-conditioned which is sensitive to roundoff errors and errors in data. In particular, for the TORC system which has an ill-conditioned linear model, controllability Gramian is a better approach for controllability analysis.

For a linear time-invariant system (3.1), if all eigenvalues of the system matrix, A, have negative real part, then the unique solution of Lyapunov equation (3.2), W_c, is positive definite if and only if the pair (A,B) is controllable.

$$AW_c + W_cA^T = -BB^T \tag{3.4}$$

W_c is known as *controllability Gramian* and can also be expressed as,

$$W_c = \int_0^\infty e^{A\tau} BB^T e^{A^T\tau} d\tau$$

Analyzing the controllability of TORC through constructing the controllability Gramian reveals that W_c is positive definite, and the system is fully controllable. This illustrates that all state variables of the system can be utilized to implement the optimal controller.

Now, the main purpose of a control system design is to regulate the system state from an arbitrary initial condition, $x(0) = x_0$, asymptotically to the state space origin as $t \to \infty$. In this control design,

the hyperplane, H, is designed such that the system states satisfy equation (3.2),

$$S \doteq \{x : h^j x = 0\}, j = 1, 2, ..., m \tag{3.5}$$

where h^j is a row n-vector and m is the number of control inputs. The subspace is the set of x which makes up S. Accordingly, the ideal case is that the system state slides over each of the defined hyperplanes, h^j. In algebraic terms, the defined subspace S is the null space of H (3.4).

$$Hx = 0, \qquad \forall t > t_s \tag{3.6}$$

where t_s is the time at which the sliding mode is reached. In fact, equation 3.4 defines a sliding motion such that once the sliding mode resides on the hyperplane, condition (3.5), derivation of sliding motion, will be equal to zero.

$$H\dot{x}(t) = 0, \qquad \forall t > t_s \tag{3.7}$$

Substitution of linear system model (3.1) gives (3.6).

$$HAx(t) + HBu(t) = 0, \qquad \forall t > t_s \tag{3.8}$$

Then, if $|HB| \neq 0$ the equivalent control will be in the linear feedback form,

$$u_{eq}(t) = -Kx(t) \tag{3.9}$$

where the feedback matrix, K, is given by,

$$K = (HB)^{-1}HA \tag{3.10}$$

Eventually, the sliding motion can be represented by the system equation as below,

$$\dot{x}(t) = A_{eq}x(t) = [I_n - B(HB)^{-1}H]Ax(t) \tag{3.11}$$

where I_n is the $n \times n$ identity matrix. According to (3.11), motion equation is independent of actual value of control, u, and only dependent on the constructed hyperplane matrix, H. In fact, the controls function is to drive and to maintain the state into S.

3.1.2 Optimal Hyperplane Design

Now, the control design is to construct a hyperplane or subspace in system state space. One method to build the hyperplane in state space is to define a quadratic cost function of state and controls so that state and control input constraints can be defined as weight matrices in the cost function. For hyperplane design, first, the linear system model is transformed into controllable canonical form by an orthogonal transformation, T, such that,

$$TB = \begin{bmatrix} 0 \\ B_0 \end{bmatrix} \tag{3.12}$$

where B_0 is an $m \times m$ non-singular matrix. Using T transformation matrix, the transformed state variable $\bar{x} = Tx$ is defined such that the linear system model can be expressed in the following form,

$$\dot{\bar{x}} = TAT^T x(t) + TBu(t) \tag{3.13}$$

Therefore, the transformed sliding condition is,

$$HT^T x(t) = 0 \tag{3.14}$$

The transformed state, $\bar{x}$, can be partitioned into two parts,

$$\bar{x} = \begin{bmatrix} \bar{x_1} & \bar{x_2} \end{bmatrix}, \quad \bar{x_1} \in \Re^{n-m}, \quad \bar{x_2} \in \Re^m \tag{3.15}$$

and the transformed linear system matrices, TAT^T, TB and CT^T, can be partitioned accordingly,

$$\dot{\bar{x_1}} = A_{11}\bar{x_1} + A_{12}\bar{x_2} \tag{3.16}$$

$$\dot{\bar{x_2}} = A_{21}\bar{x_1} + A_{22}\bar{x_2} + B_0 u(t) \tag{3.17}$$

and,

$$H_1\bar{x_1} + H_2\bar{x_2} = 0 \tag{3.18}$$

where,

$$TAT^T = \begin{bmatrix} A_{11} & A_{12} \\ A_{21} & A_{22} \end{bmatrix}; \quad HT^T = [H_1 \; H_2] \tag{3.19}$$

Now, the hyperplane design problem is reduced to selecting H_1 and H_2. In this regards, recall the assumption that the product matrix HB is nonsingular ($|HB| \neq 0$) such that,

$$|H_2 B_0| = |HT^T.TB| = |HB| \neq 0 \tag{3.20}$$

This implies that the $m \times m$ matrix H_2 must be non-singular, $|H_2 B_0| \neq 0$. In other words, according to the sliding condition 3.18, $\bar{x_2}$ is dependent on $\bar{x_1}$ so that there is an $m \times m$ degree of freedom in selection of the hyperplane, H. Thus, H_2 can be chosen in such a way that it reduces computational burden. In the case of being B_0 nonsingular, the appropriate choice is an $m \times m$ identity matrix, I_m such that $H_2 = I$.

Restating the hyperplane design problem, the ideal control such that the state slides over the hyperplane according to sliding mode condition (3.18) is formulated as below,

$$\dot{\bar{x_1}}(t) = A_{11}\bar{x_1}(t) + A_{12}\bar{x_2}(t) \tag{3.21}$$

$$\bar{x_2}(t) = -H_1\bar{x_1}(t) \tag{3.22}$$

In other words, the hyperplane design problem is transformed into a linear state feedback problem such that x_2 act as controls of the $m \times n$ subsystem where x_1 is the subsystem's state variable. Hence, the closed loop system will be,

$$\dot{\bar{x_1}}(t) = (A_{11} - A_{12}H_1)\bar{x_1}(t) \tag{3.23}$$

where H_1 is the state feedback gain matrix and $H = [H_1\ I_m]T$.

to design the optimal hyperplane in system state space, a cost function , J, is defined where it put constraints on the state variable.

$$J = \frac{1}{2}\int_0^\infty (x^T Q x)\, dt \tag{3.24}$$

where Q is a diagonal matrix defined based on state variable constraints, which is that each diagonal element related to a state variable is determined by the permissible deviation of the state variable

from its nominal value. If the cost function is expressed in the transformed state form, it will be as below,

$$J = \frac{1}{2}\int_0^\infty \bar{x}_1^T Q_{11}\bar{x}_1 + 2\bar{x}_1^T Q_{12}\bar{x}_2 + \bar{x}_2^T Q_{22}\bar{x}_2 \, dt \tag{3.25}$$

where,

$$TQT^T = \begin{bmatrix} Q_{11} & Q_{12} \\ Q_{21} & Q_{22} \end{bmatrix} \tag{3.26}$$

given that, $Q_{12} = Q_{21}^T$.

Solving this LQR problem leads to the calculation of an optimal state feedback gain, K_0, where this gain is utilized as an initial guess for calculation of H_1. The derived gain, K_0, from the initial LQR problem is used to design the final optimal hyperplane such that another LQR problem is solved through defining a normalized quadratic cost function where it puts constraints on control as well as state variables.

$$J = \frac{1}{2}\int_0^\infty x Q x^T + u_{eq} R u_{eq}^T dt \tag{3.27}$$

where Q is defined same as last LQR problem multiplied by a tuning parameter to normalized the quadratic cost function such that R becomes an 2×2 identity matrix. Also, $u_{eq}(t) = -Kx(t)$ (3.9) and $K = (HB)^{-1}HA$ (3.10). Substitution of (3.19) provides,

$$\begin{aligned} J = \frac{1}{2}\int_0^\infty \quad & \bar{x}_1 \left[Q_{11} + (H_1A_{11} + A_{21})^T F (H_1A_{11} + A_{21})\right] \bar{x}_1^T + \\ & 2\bar{x}_1 \left[Q_{12} + (H_1A_{11} + A_{21})^T F (H_1A_{12} + A_{22})\right] \bar{x}_2^T + \\ & \bar{x}_2 \left[Q_{22} + (H_1A_{12} + A_{22})^T F (H_1A_{12} + A_{22})\right] \bar{x}_2^T \, dt \end{aligned} \tag{3.28}$$

where $F = (B_0^{-1})^T R B_0^{-1}$.

Solving the second LQR problem leads to the calculation of the final H_1 where this will make the optimal hyperplane in the system state space, H, through minimizing the cost function (3.27).

Recalling equation (3.9), (3.19) and (3.10) provides the optimal control as below,

$$u_{eq} = -Kx(t) \tag{3.29}$$

$$K = (HB)^{-1}HA \tag{3.30}$$

$$H = \begin{bmatrix} H_1 & I \end{bmatrix} T \tag{3.31}$$

3.1.3 Robust Control

After designing the optimal hyperplane, a robust term is needed such that it guarantees that the system slides over the optimal hyperplane. Therefore, Lyapunov stability theory provides a ground on how to robustify the control design. In this regards, a Lyapunov function candidate is chosen as below,

$$V_i = \frac{1}{2} S_i^T S_i, \qquad i = 1,2 \tag{3.32}$$

$$S_i = H_i x(t), \qquad i = 1,2 \tag{3.33}$$

Thus,

$$V_i = \frac{1}{2} x^T H_i^T H_i x, \qquad i = 1,2 \tag{3.34}$$

According to Lyapunov stability theory, the time derivative of positive definite Lyapunov function must be $\dot{V} \leq 0$ to guarantee the stability of the system.

$$\dot{V}_i = \overbrace{x^T H_i^T}^{S_i^T} \overbrace{H_i \dot{x}}^{\dot{S}_i}, \qquad i = 1,2 \tag{3.35}$$

$$\dot{V}_i = x^T H_i^T H_i \left(Ax + Bu + f(x,u)\right) \tag{3.36}$$

where $f(x,u) \leq F$ represents the model uncertainties and nonlinearities and F is a boundary. Thus, to achieve $\dot{V} = S^T \dot{S} \leq 0$, S and $\dot{S}$ must have an opposite sign so that feedback controls, u plays an essential role to determine the sign of $\dot{S}$. Therefore, a robust term, $\zeta(t)$ must be introduced such that it leads $\dot{S}$ in opposite direction of S. Combining such robust term into the ideal control results in the robust control law as follows,

$$u^{\star}(t) = -Kx(t) + \zeta(t) \tag{3.37}$$

therefore, substitution of (3.37) into (3.37) gives,

$$\dot{V}_i = x^T H_i^T H_i (A - BK)x + x^T H_i^T H_i f + X^T H_i^T H_i B\zeta, \quad i = 1,2 \tag{3.38}$$

Recall (3.30) so that,

$$\dot{V}_i = x^T H_i^T H_i Ax - x^T H_i^T H_i B(H_i B)^{-1} H_i Ax + x^T H_i^T H_i f + x^T H_i^T H_i B\zeta, \quad i = 1,2 \tag{3.39}$$

After simplification of (3.39, the first two terms cancel out each other in the converging phase and the remaining is,

$$\dot{V} = x^T (H_i^T H_i f + H_i^T H_i B\zeta), \qquad i = 1,2 \tag{3.40}$$

Recall that the multi-product matrix, H_iB, is nonsingular, so that ζ must have an opposite sign to $S^T = x^T H_i^T$ to make the second term negative so that selecting proper boundary for ζ guarantees bounded stability. To choose a robust term, $\zeta(t)$, a sign function of S, $sgn(S)$, can be chosen to guarantee the stability, but it results in chattering of the controls, u. The chatter of actuators is quite damaging in ORC system applications, so that the smoothing control introduced in introduction chapter is done by a saturation function of S, $sat(S)$ to tackle the chattering problem. Figure 3.1) illustrates a saturation function.

$$\zeta(t) = sat(S_i) = \begin{cases} -b, & S_i \geq b \\ S_i, & -b < S_i < b \\ b, & S_i \leq -b \end{cases} \tag{3.41}$$

where b is a constant positive vector represents boundary of the saturation function. The boundary parameter must be chosen properly such that it does not allow the system deviates from the optimal hyperplane in the system state space. Therefore, if $b \geq F$, bounded stability is guaranteed such that,

$$\dot{V}_i \leq \|x\|(F - b), \qquad \|S_i\| \geq b \tag{3.42}$$

On the other hand, an issue is the bigger b, the more vulnerable to chatter.

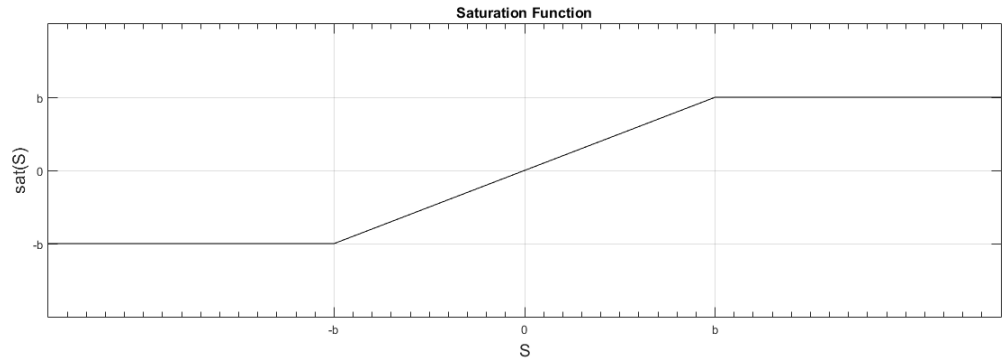

Figure 3.1: saturation function

To sum up, a robust optimal control was designed in this section, but the problem is that if the bound parameter of the saturation function is chosen too big, the system is susceptible to chatter, and if the boundary parameter is chosen too small relative to disturbances and uncertainties, it dose not guarantee robustness of the control system. Hence, in which significant model uncertainties and disturbances are involved in a system, a solution is that a new term in control law is introduced such that it adapts to the amount of the uncertainties online. Next section will address this issue using a neural network technique.

3.2 Adaptive CMAC Neural Networks Design

Tuning of the robust term, $\zeta(x)$ is problematic in VSC design because it is proportional to the disturbances and uncertainties into the controlled system. Thus, if the robust term is too small, the stability of the closed-loop system will not be guaranteed. On the other hand, if the the robust term is too large, chattering will be observed. Therefore, an adaptive term can be added to the control law to cancel out the effect of disturbances and uncertainties.

Kim *et al.* [43] proposed an intelligent optimal state feedback control using a neural network technique called Cerebellar Model Arithmetic Computer (CMAC). The proposed controller integrated a linear optimal control and neural network learning methods. The neural network was used to improve performance in the case of uncertainties and disturbances. There are other works

that combined optimal control strategy with intelligent control methods to improve performance [44, 45, 46, 47]. Also, integration of intelligent control technique such as fuzzy logic or neural networks- with VSC has shown promising improvement in dealing with complex and uncertain systems [48]. Al-Holou *et al.* introduced a sliding mode neural network fuzzy logic control with application in active suspension systems to enhance the ride and comfort.

In particular, CMAC neural network first proposed by Albus 1975 [49] where CMAC has a similar architecture to Radial Basis Function network (RBFN). Similar to RBFN, CMAC is among the category of associative memory neural networks. Originally, CMAC is inspired from the structure of particular part of the brain known as the cerebellum. CMAC has shown better performance than RBFN. Taghavipour [50] compared CMAC with RBFN in a hydraulic hybrid vehicle application. CMAC showed better performance over RBFN proofing higher performance of CMAC. Moreover, the curse of dimensionality problem is inevitable in RBFN when the number of neural network inputs goes beyond 4. Kretchmar 1997 [51] examined the similarity and difference of CMACs and RBFNs thoroughly in which the curse of dimensionality problem in RBFN was explained in detail. Comparing CMAC and RBFN with another neural network technique, they exhibit faster convergence/adaptation than the well-known multilayer perceptron back-propagation (MLP) networks so that this characteristic makes CMAC suitable for online adaptation in control design applications especially in which the convergence speed is of high importance rather than accuracy. In this work, an optimal VSC integrated with CMAC neural networks is proposed to cancel out uncertainties and disturbances in an adaptive way.

First, the control system architecture using CMAC will be introduced to provide an overview regarding CMAC adaptive control design. Then, CMAC adaptation law will be derived based on Lyapunov stability analysis such that a Lyapunov function candidate based on energy components of the system will be proposed to design a stable CMAC neural network architecture.

3.2.1 CMAC Neural Networks Architecture

The aim of this section is to make the designed robust optimal control system architecture adaptive to disturbances. Therefore, the robust term presented in last section must be adaptive to the disturbances which deviate the system state from sliding over the optimal hyperplane. The idea is to utilize CMAC neural networks as an adaptive term of the control law where the neural networks can learn online through feeding the neural networks with the system state. Furthermore, neural network weights are updated at specific intervals in such a way that the weights are updated based on penalizing the adaptive term for deviating from the sliding condition (3.6).

As an introduction on CMAC neural networks, CMAC architecture is similar to Radial Basis Function networks (RBFN) consisting of a weighted sum of basis functions,

$$\hat{f}(q) = \hat{W}^T \Phi(q)$$

where $q \in \Re^n$ contains inputs, Φ is a row vector of basis functions which is spline function in this work, and w is a column vector of weights. As shown in figure 3.2, the spline function is governed by a polynomial presented at (3.43) [52].

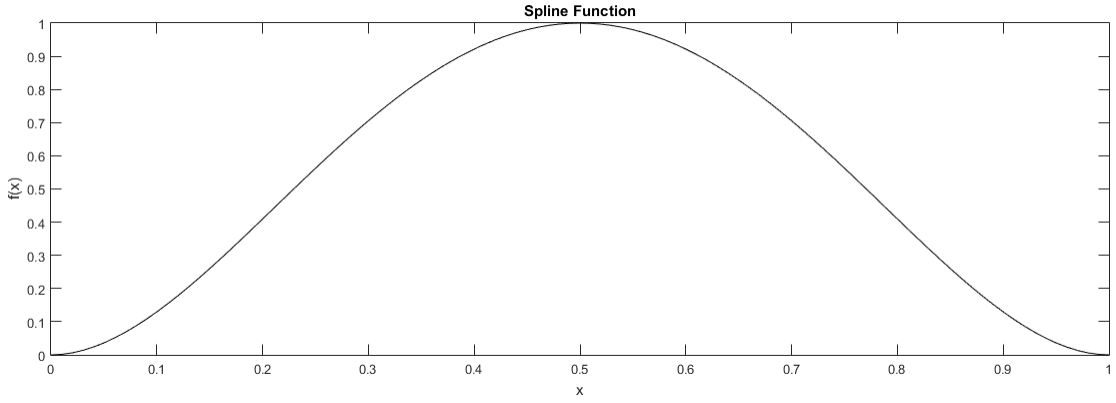

Figure 3.2: spline function

$$y = 16\,(x^2 - 2x^3 + x^4) \tag{3.43}$$

The input space is divided into Q hypercubes per input, each of which is associated with a memory cell. The memory cells contain weights which are updated during training in each update interval. Moreover, there are L layers of the input space quantification so that any point in input space is associated with L memory cells. Finally, CMAC output is a weighted sum of basis functions in each layer activated by the input. Thus, the total number of cells in CMAC architecture is LQ^n where only L basis function need to be calculated in each interval. This is an advantage of CMAC in comparison with RBFN since the number of basis function calculations increases exponentially with the number of inputs in RBFN. Figure 3.3 illustrates two examples of one-dimensional and two-dimensional CMAC with spline basis functions.

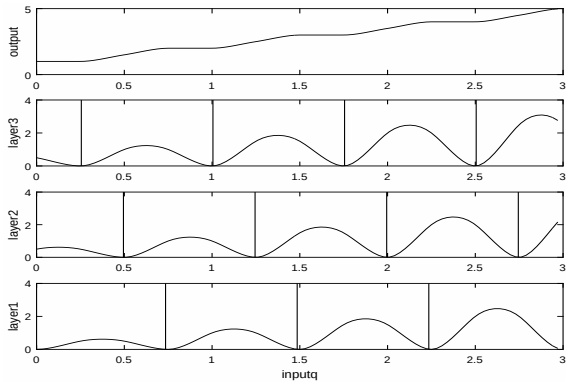

(a) CMAC with spline basis functions, n=1 input, L=3 layers, and Q=5 quantifications

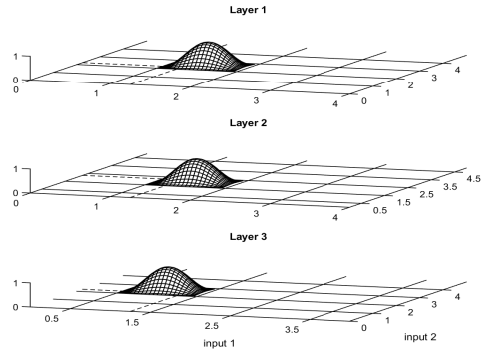

(b) CMAC with spline basis functions, n=2 inputs, L=3 layers, and Q=5 quantifications (only the activated basis functions indexed by the input are shown)

Figure 3.3: spline CMAC examples

CMAC can be utilized as a real-time universal nonlinear approximator such that it is capable of approximation of a nonlinear function, $f(q)$, through some training intervals.

$$f(q) = W^T \Phi(q) + \varepsilon(q), \quad ||\varepsilon(q)|| \leq \varepsilon_{max} \quad \forall q \in D, \tag{3.44}$$

where $\varepsilon(q)$ represents the approximation error in the uniform approximation region $D \subset \Re$ where $\varepsilon(q)$ is bounded by known constant ε_{max}. In this notation, W contains ideal weights whereas $\hat{W}$

represents the weight estimates so that there is a weight error denoted by $\tilde{W}$,

$$\tilde{W} = W - \hat{W} \tag{3.45}$$

Therefore, if CMAC output which is approximated nonlinear function is denoted by $\hat{f}(q)$, approximation error of the nonlinear function can be represented as below,

$$f(q) - \hat{f}(q) = \left[W^T \Phi(q) + \varepsilon(q)\right] - \hat{W}^T \Phi(q) = \tilde{W}^T \Phi(q) + \varepsilon(q) \tag{3.46}$$

In this work, CMAC is utilized to approximate disturbances, model uncertainties, external disturbances and nonlinearities assuming all accumulated in control input channel denoted by a 2×2, $f(x)$ matrix. Hence, the state space representation of TORC system can be formulated as follows,

$$\dot{x}(t) = Ax(t) + B\left[u^\star(t) + f(x)\right] \tag{3.47}$$

where $f(x) = (HB)^{-1} f'(x)$ such that according to (3.20), HB is a nonsingular and invertible matrix which maps model uncertainties onto the control. Also, $f'(x)$ is a 2×2 matrix represents model uncertainties. Now, control law is introduced using CMAC neural network term,

$$u(t) = -Kx(t) + \zeta(x) - \hat{W}^T \Phi \tag{3.48}$$

substitution of (3.48) into (3.47) using (3.44) gives,

$$\dot{x}(t) = (A - BK)x(t) + B\zeta(t) + B\left[W^T \Phi(x) + \varepsilon(x) - \hat{W}^T \Phi\right] \tag{3.49}$$

According to (3.44), CMAC approximation error of the nonlinear function $f(x)$ can be represented by $[\tilde{W}^T \Phi(x) + \varepsilon(x)]$ so that the system error dynamics becomes,

$$\dot{x}(t) = (A - BK)x(t) + B\zeta(t) + B\tilde{W}^T \Phi(x) + B\,\varepsilon(x). \tag{3.50}$$

To make best use of CMAC, an appropriate weight update law, $\dot{\hat{w}}$, must be formulated such that estimation error converges to zero as time goes by. In this regards, Lyapunov stability theory is used

by selecting a Lyapunov function representing energy components of the system. An appropriate Lyapunov function candidate consists of quadratic term of the designed optimal hyperplane and the weight error,

$$V = \frac{1}{2} S^T S + \frac{1}{2\beta} tr(\tilde{W}^T \tilde{W}) \tag{3.51}$$

where $tr(\cdots)$ denotes matrix trace. Since energy elements of the weight error are accumulated on the main diagonal, the trace of quadratic term of weight error is a proper candidate for Lyapunov function. Now, substitution of $S = Hx$ into (3.51) will result in,

$$V = \frac{1}{2} x^T H^T H x + \frac{1}{2\beta} tr(\tilde{W}^T \tilde{W}) \tag{3.52}$$

The Lyapunov function representing the energy components of the system must decrease all through the time to guarantee the stability of the control system so that $\dot{V} < 0$,

$$\dot{V} = x^T H^T H \dot{x} + \frac{1}{\beta} tr(\tilde{W}^T \dot{\tilde{W}}) \tag{3.53}$$

recall $\tilde{w} = w - \hat{w}$, so that,

$$\dot{\tilde{w}} = 0 - \dot{\hat{w}}$$

recall the error dynamics (3.48) and substitute into (3.53) results in,

$$\dot{V} = x^T H^T H \left[(A - BK)x(t) + B\zeta(t) + B\tilde{W}^T \Phi(x) + B\varepsilon(x) \right] - \frac{1}{\beta} tr(\tilde{W}^T \dot{\hat{W}}), \tag{3.54}$$

Then,

$$\dot{V} = x^T \left[H^T H (A - BK) \right] x + x^T H^T H B \zeta(x) + x^T H^T H B \varepsilon(x) + x^T H^T H B (\tilde{W}^T \Phi) - \frac{1}{\beta} tr(\tilde{W}^T . \dot{\hat{W}}) \tag{3.55}$$

Recall $H = \begin{bmatrix} H_1 & I \end{bmatrix} T$, so that

$$HB = \begin{bmatrix} H_1 & I \end{bmatrix} T B = \begin{bmatrix} H_1 & I \end{bmatrix} \begin{bmatrix} 0 \\ B_0 \end{bmatrix} = B_0.$$

Therefore,

$$\dot{V} = x^T \left[H^T H (A - BK) \right] x + x^T H^T B_0 \zeta(x) + x^T H^T B_0 \varepsilon(x) + x^T H^T B_0 (\tilde{W}^T \Phi) - \frac{1}{\beta} tr(\tilde{W}^T \dot{\hat{W}}). \tag{3.56}$$

According to (3.40), $H^T H\,(A-BK)=0$ so that,

$$\dot{V}=x^T H^T B_0\zeta(x)+x^T H^T B_0\,\varepsilon(x)+tr\left(\tilde{W}^T\left(\Phi B_0^T Hx-\frac{1}{\beta}\dot{\hat{W}}\right)\right) \tag{3.57}$$

Given that the Lyapunov stability condition, $\dot{V}\leq 0$, must be met and the stability of the VSC has already been investigated in last section, $x^T H^T\,\zeta(x)$ is negative semi-definite and the last term representing the energy components of the weight error is for what CMAC control design is concerned. To satisfy the Lyapunov stability condition, the weight update law, $\dot{\hat{W}}$, is selected in such a way that non-negative definite term, $x^T H^T B_0\,(\hat{W}^T\Phi)$ is canceled out. Thus, the weight update law is introduced as below,

$$\dot{\hat{W}}=\beta\left(\Phi B_0^T H x-\nu\,\|x\|\,\hat{W}\right) \tag{3.58}$$

where the term, $\nu\|x\|\hat{W}$, is a robust term called *e-modification* which prevents the weight drift toward instability [52]. Also, ν is a constant vector for tuning of the robust term, and β is a tuning parameter which denotes neural network weight update speed or adaptation rate. Now substitution of 3.58 into 3.57 results in,

$$\dot{V}=x^T H^T B_0\,\zeta(x)+x^T H^T B_0\,\varepsilon(x)+tr\left(\tilde{W}^T\left(-\nu\,\|x\|\,\hat{W}\right)\right). \tag{3.59}$$

Given that $\zeta(x)$ has an opposite sign of $x^T H^T$, the first term is negative so that the following inequality can be obtained using 3.45 in the region $\|S\|\geq b$,

$$\dot{V}\leq-\|x\|\,\zeta_{max}+\|x\|\varepsilon_{max}+\nu\,\|x\|\,\left(\|\tilde{W}\|_F W_F-\|\tilde{W}\|_F^2\right),\quad \|S\|\geq b \tag{3.60}$$

where the following inequality is utilized using Frobenius norm,

$$tr(\tilde{W}^T(W-\tilde{W}))=\left\langle\tilde{W},W\right\rangle_F-\|\tilde{W}\|_F^2\leq\left(\|\tilde{W}\|_F W_F-\|\tilde{W}\|_F^2\right) \tag{3.61}$$

Now, completing the square terms gives,

$$\dot{V}\leq-\|x\|\left[\zeta_{max}-\varepsilon_{max}+\nu\left(\|\tilde{W}\|_F-\frac{1}{2}W_F\right)^2-\frac{1}{4}\nu W_F^2\right],\quad \|S\|\geq b \tag{3.62}$$

which shows whenever $\|S(0)\| > b$, $\|S(t)\|$ will be strictly decreasing until it reaches the set $\left\{ \|S\| \leq b \right\}$ in finite time and remains inside thereafter, such that,

$$\|x\| \geq \frac{\varepsilon_{max} + \frac{1}{4}\nu W_F^2}{\zeta_{max}} \equiv B_x \qquad \|\tilde{W}\|_F \geq \sqrt{\varepsilon_{max} + \frac{1}{4}\nu W_F^2} + \frac{1}{2}W_F \equiv B_w \tag{3.63}$$

where B_x and B_w are the convergence region or boundary layer, and it demonstrates *Uniformly Ultimately Boundedness* (UUB) of $x(t)$ and $\tilde{W}(t)$.

Aside from the Lyapunov stability analysis, the objective is to slide over the optimal hyperplane, and the sliding condition or performance criteria is $Hx(t) = 0$ so that this term in weight update law penalizes the neural network weights if they deviate from the sliding condition. To sum up, the CMAC neural networks combined with the optimal control is contributed to an adaptive optimal control system design. Hence, the controlled system can slide over the optimal hyperplane in the system state space despite the fact that disturbances, model uncertainties, and nonlinearity must be canceled out such that the nominal optimal controller maintains its nominal performance through set-point tracking and disturbance rejection.

3.3 Kalman Filter Optimal State Estimator Design

This section addresses as issue in previous control system design which is that some of the system states are not measurable. The lack of full measurement data can be solved by an state estimator so that Kalman Filter (KF) [35] is utilized. KF is a powerful tool for state estimation as the sensor measurement noise, model uncertainties and disturbances are considered in KF design. Furthermore, ORC system is a relatively slow dynamic system in comparison with robotic applications such that it enables using a fast dynamic or high gain estimator regardless of the model accuracy.

KF design is quite similar to an LQR problem as a cost function is defined where model uncertainties, disturbances and measurement noise is taken into account. This optimization problem

is solved through solving an Algebraic Riccati Equation (ARE). It is worth mentioning that the measurement noise is assumed as white noise in KF design. To design a KF, the linear model of the system is considered as below,

$$\dot{x}(t) = Ax(t) + B_1 u(t) + B_2 w(t) \tag{3.64}$$

$$y(t) = Cx(t) + v(t) \tag{3.65}$$

where $x(t) \in \Re^n$ and $u(t) \in \Re^m$ are system state and controls respectively, $w(t) \in \Re^n$ contains model uncertainties, and disturbances, $y(t) \in \Re^p$ is the measurement output, and $v(t) \in \Re^p$ is the white noise added to the measurement output. w and v are assumed to be uncorrelated zero-mean Gaussian stochastic processes so that,

$$E[w(t)] = 0 \qquad E[v(t)] = 0 \qquad E\left[w(t)\, v^T(t)\right] = 0 \tag{3.66}$$

$$E\left[w(t)\, w^T(t)\right] = Q_{est}\, \delta(t-\tau) \qquad E\left[v(t)\, v^T(t)\right] = R_{est}\, \delta(t-\tau) \tag{3.67}$$

where δ is Dirak delta function. T here are two approaches for KF design, stochastic and deterministic. In this work, the deterministic interpretation of the KF design is used so that the process is similar to LQR problem. The KF dynamic model is formulated as below,

$$\dot{\hat{x}}(t) = A\hat{x}(t) + Bu(t) + L(y(t) - C\hat{x}(t)) \tag{3.68}$$

Or,

$$\dot{\hat{x}}(t) = (A - LC)\hat{x}(t) + B\,u(t) + L y(t) \tag{3.69}$$

where $\hat{x} \in \Re^n$ is the state estimate vector and L is the KF gain. Now, the KF design can be cast as an optimization problem to calculate L in such a way that (3.69) is stable. First, a cost function is defined such that the model uncertainties, disturbances, and sensor noise is taken into account,

$$J_e = \frac{1}{2}\int_0^\infty \tilde{x}^T Q_{est} \tilde{x} + v^T R_{est} v, \tag{3.70}$$

where,

$$\tilde{x} = x - \hat{x}.$$

To minimize the defined cost function, the ARE (3.71) is solved,

$$AS + SA^T - SC^T R_{est} CS + Q_{est} = 0 \tag{3.71}$$

where S solves the ARE, and S is used to calculate the KF gain, L such that,

$$L = SC^T R_{est}^{-1} \tag{3.72}$$

L makes the optimal observer stable as long as the pair of (A^T, C^T) is stabilizable, and the pair of $(A^T, Q_{est}^{\frac{1}{2}})$ is detectable.

3.4 Adaptive Variable Structure Control

This section combines all previous designs into an adaptive variable structure controller (AVSC). In CMAC design section, The designed optimal controller was combined with CMAC to make the optimal controller adaptive to disturbances and uncertainties. In this regards, all states have to be measurable such that state error can be used for CMAC weight updates. However, measurements of all state variables are viable but not cost-effective. Therefore, a Kalman filter was designed for state estimation so that given output variables, all the state variables can be estimated by the Kalman filter.

To reach this goal, the control law is modified as below,

$$u(t) = -K\hat{x}(t) + \zeta(t) - \tilde{W}^T \Phi \tag{3.73}$$

where $\hat{x}(t)$ is the state estimate calculated by Kalman filter. Furthermore, CMAC weight update law must be modified accordingly, which is represented as below,

$$\dot{\hat{W}} = \beta \left(\Phi B_0^T H \hat{x} - \nu \|\hat{x}\| \hat{W} \right) \tag{3.74}$$

It is worth restating that CMAC weight is updated each 0.2 second whereas time step is 0.1 second in this work.

Chapter 4

SIMULATION RESULT OF DESIGNED CONTROLLER

This chapter presents simulation results of the designed controllers in TORC system such that set-point tracking and disturbance rejection are examined as fundamental performance indicators in control systems. In this regards, first CMAC neural network adaptability are tested such that parameters of CMAC are tuned to achieve a fast and stable convergence. Then, set-point tracking and disturbance rejection performance of AVSC control are compared with VSC. Furthermore, AVSC is compared with well-known H_∞ control where H_∞ control is considered as a robust control strategy where it relies on linear model. In addition, H_∞ synthesis is briefly explained such that features of H_∞ control as well as tuning parameters are pointed out. Ultimately, AVSC is compared with the industrial accepted PI control where it is tuned by IMC-PID tuning rules.

4.1 Adaptive Variable Structure Control Performance

The designed control consisting of the VSC term $(-Kx+\zeta(x))$ and the CMAC neural network term $(W^T\Phi)$ is tuned such that the VSC control does not cause chattering problem since chattering must be avoided in this industrial application. First, the diagonal Q, matrix in the normalized cost function is tuned in such a way that the allowable state variation is embedded into that as follows,

$$q_{ii} = \frac{1}{\Delta x_i}, \qquad i = 1,\ldots,13$$

As this is a normalized cost function, R is a 2×2 identity matrix and Q is multiplied by a constant, r, which is tune according to allowable variations of MVs. Thus, the optimal hyper plane in the system state space is derived through solving two LQR problem explained in the hyper plane design section, and using the calculated optimal hyper plane, K is calculated by 3.32.

Furthermore, the same method is used to tune diagonal matrix, Q_est in the normalized cost function of the Kalman filter design. Then, unmeasurable estimated states are substituted into the control law.

Now that the VSC term is calculated, the adaptive CMAC neural network term in control law must be tuned to achieve a fast and stable convergence. First, the control loop time step and CMAC training intervals are chosen. The control loop time step is 0.1 second whereas the neural network term in control law, $\tilde{W}^T \Phi$, updates every 0.2 second due to the slow dynamic nature of disturbance and lower computational burden. In addition, the best practice to choose a time step is that the time step should be 10 times per process time constant. According to the simulation results, the process dominant time constant of the studied TORC system is approximately 8 seconds so that 0.1 second time step is a prudent choice. Then, the parameters of CMAC neural networks are tuned as follows,

$$N = 6, \quad Q = 10, \quad L = 60, \quad \beta = \begin{bmatrix} 10 \\ 15 \end{bmatrix} \times 10^{-2}, \quad \nu = \begin{bmatrix} 10^{-6} \\ 10^{-6} \end{bmatrix}$$

where N is the number of CMAC inputs which partial state variables are used to reduce computational burden. Q is the quantification number showing the hypercubes per input; L is the number of layers or number of basis functions; β is CMAC the weigh update rate where it is tuned in such a way that aggressive weight update is not observed; ν is the robust term constant in weight updates law.

Now that all terms of AVSC are tuned, the disturbance rejection and set-point tracking performance can be examined so that sine wave disturbance to heat source is considered in two scenarios:

1. Disturbance to heat source where control variables track a constant set-point as their nominal operating conditions,

2. Disturbance to heat source where control variables track a trajectory.

4.1.1 Disturbance Rejection Performance in Constant Operating Conditions

Recalling the control design objectives, an essential test is to examine how well the controller can reject the disturbances. According to adaptability of the designed controller, the controller are trained by different disturbance scenarios. The disturbances including fluctuation of heat source temperature and mass flow rate consist of various frequencies. In this test, sine wave disturbances shown in figure 4.1 are imposed to the system where the control objective is to maintain CVs at their nominal operating conditions. Figure 4.1 shows sine wave disturbances to heat source in 3 difference scenarios for 300 seconds which is considered as one trial epoch:

1. 1° sine wave disturbance with frequency of 0.1 rad/sec to heat source temperature when $t < 100$ seconds.

2. 0.05 Kg/sec sine wave disturbance with frequency of 0.1 rad/sec to heat source mass flow rate when $100 < t < 200$ seconds.

3. 1° sine wave disturbance with frequency of 0.1 rad/sec to heat source temperature and 0.05 Kg/sec sine wave disturbance with frequency of 0.1 rad/sec to heat source mass flow rate when $200 < t < 300$ seconds.

These disturbances are not only external disturbances but they also contribute to changing system parameters. The most important change is attributed to heat transfer coefficients of evaporator which are sensitive to mass flow rate and temperature according to modeling chapter 2.1.4. Therefore, the disturbances result in model uncertainties.

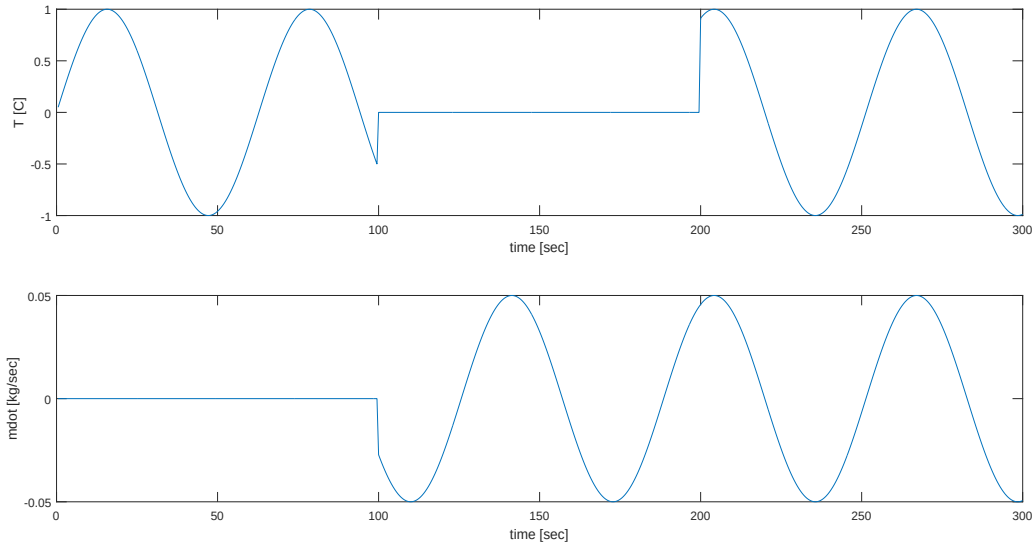

Figure 4.1: 3 different sine wave disturbance scenarios to heat source temperature and heat source mass flow rate

After 50 trials through the imposition of these situations, figure 4.2 illustrates weight convergence of CMAC neural networks where they adapt to the disturbances such that the CMAC term in control law can cancel out the effect of these disturbances. Moreover, figure 4.3 shows RMS error calculated by:

$$RMS = \left(\frac{1}{n} \sum_{i=1}^{n} (y_i^d - y_i)^2 \right)^{\frac{1}{2}} \tag{4.1}$$

where y_i^d is the desired output and n is the number of trials.

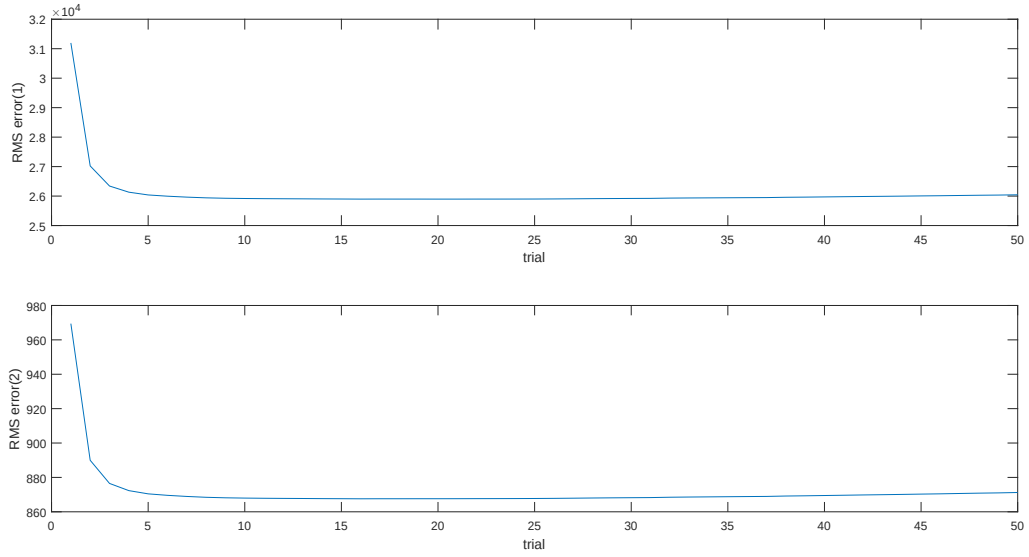

Figure 4.2: RMS error of each channel versus trials

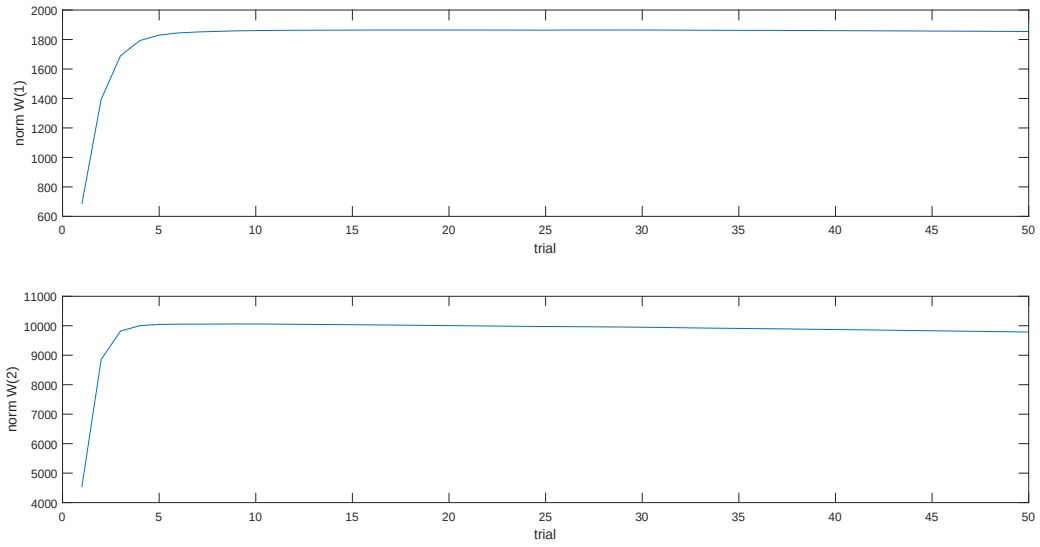

Figure 4.3: convergence of norm of weights versus trials

Figure 4.4 shows CVs where the disturbance rejection of AVSC in last training is compared with VSC revealing that adaptability of CMAC neural network integrated into VSC has improved the disturbance rejection performance and robustness margin of VSC design. Moreover, integra-

tion of CMAC neural networks into VSC design results in smoother control which is desired for this application where figure 4.5 compares MVs of AVSC and VSC design.

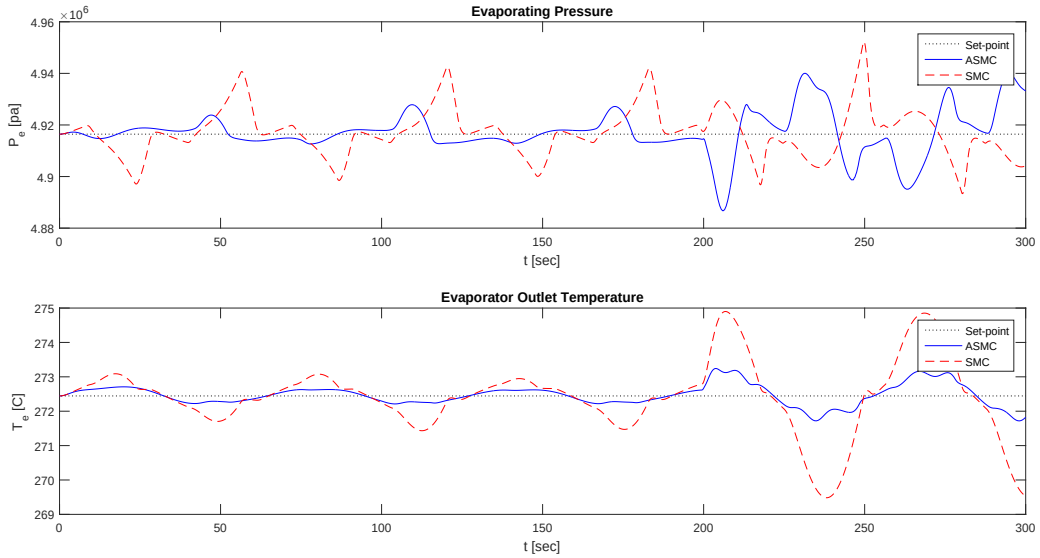

Figure 4.4: comparison of disturbance rejection performance between AVSC and VSC in constant set-point

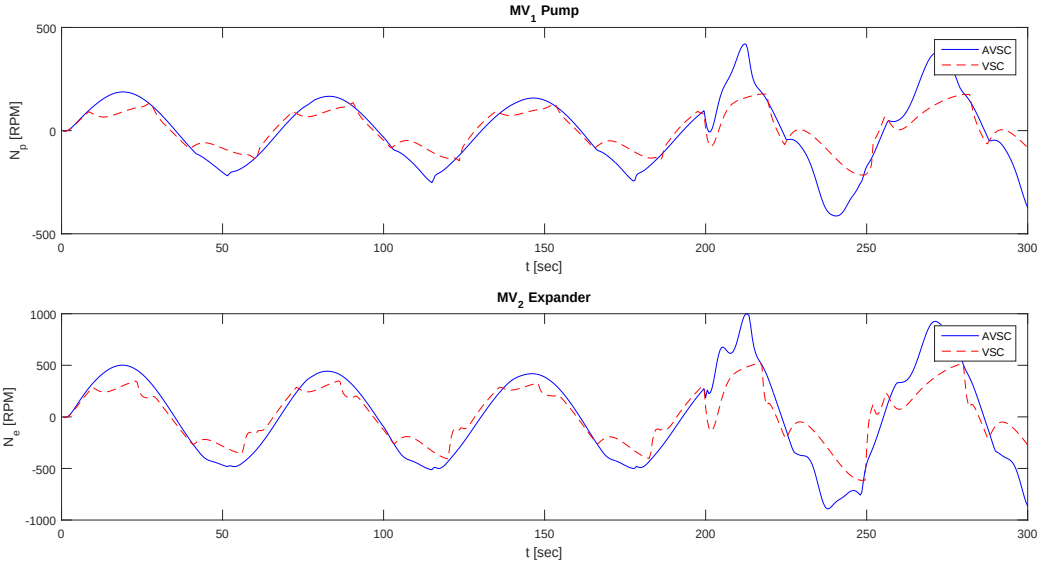

Figure 4.5: comparison of MVs between AVSC and VSC in constant set-point

In addition, figure 4.6 illustrates the CMAC neural networks outputs in the last training interval. According to the control law, the adapted CMAC output is subtracted from the VSC output contributing to canceling out the effect of disturbances and uncertainties.

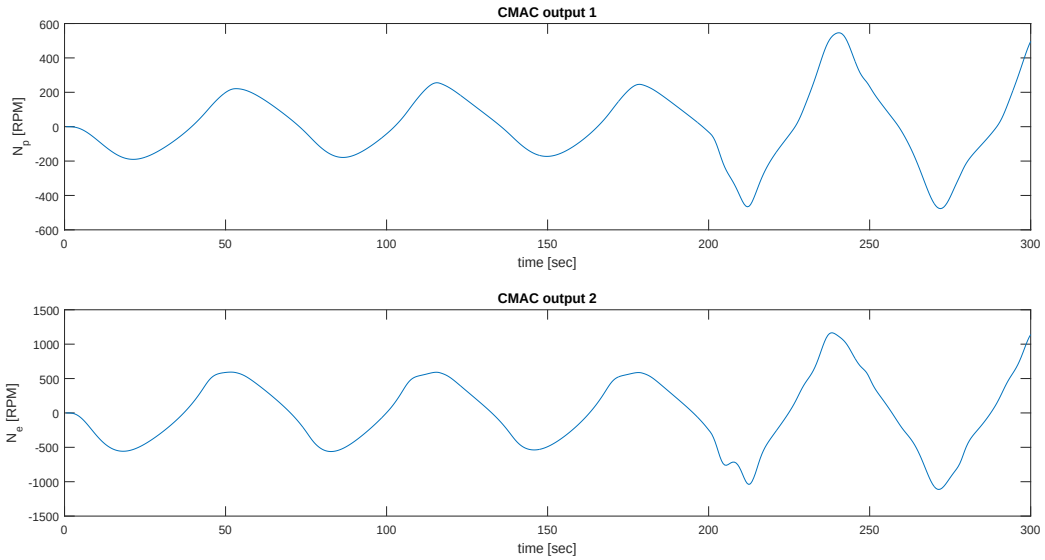

Figure 4.6: CMAC outputs

Furthermore, sliding mode condition, $Hx = 0$, is another performance indicator which reveals that integration of CMAC neural networks into VSC has improved the disturbance rejection performance. Figure 4.7 illustrates that system state can slide along the optimal hyperplane with a smaller error.

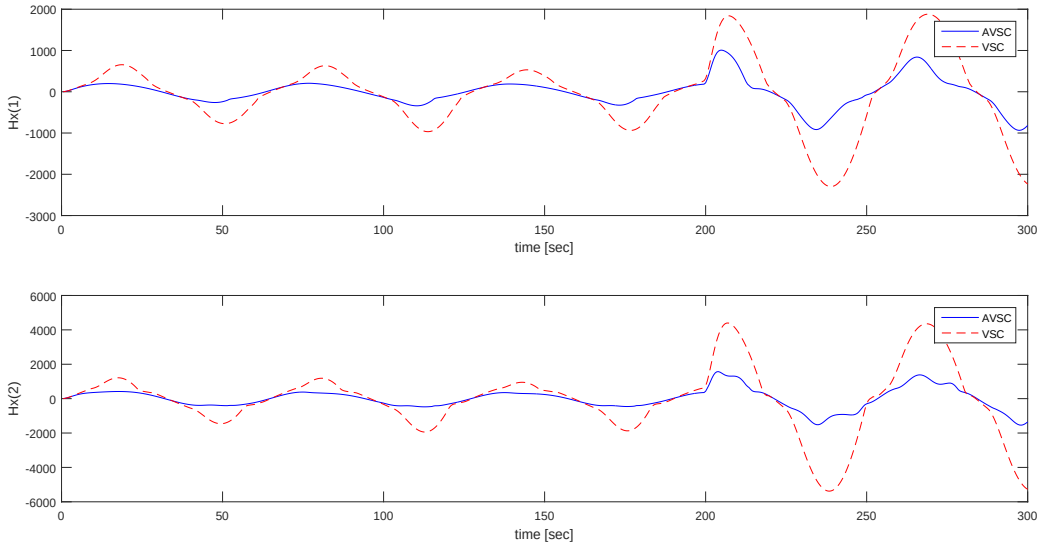

Figure 4.7: comparison of sliding mode performance between AVSC and VSC

4.1.2 Set-point Tracking Performance

After training the CMAC neural network by three disturbance scenarios, the same CMAC weights are utilized as initial CMAC weights for set-point tracking. In this test, ramp set-point changes in 250 seconds periodic interval are chosen as CMAC training epoch while the last disturbance scenarios are still imposing. Therefore, the CMAC should adapt to the new operating conditions where figure 4.8 shows weight convergence of CMAC and figure 4.9 the RMS error convergence for the new operating conditions in 10 trials.

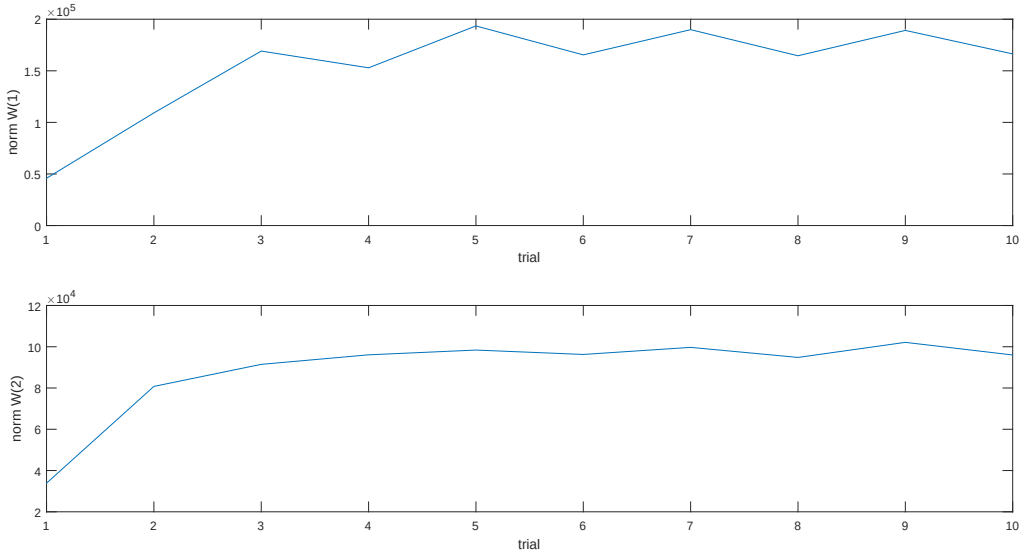

Figure 4.8: CMAC weight convergence for new set-point changes in 10 trials

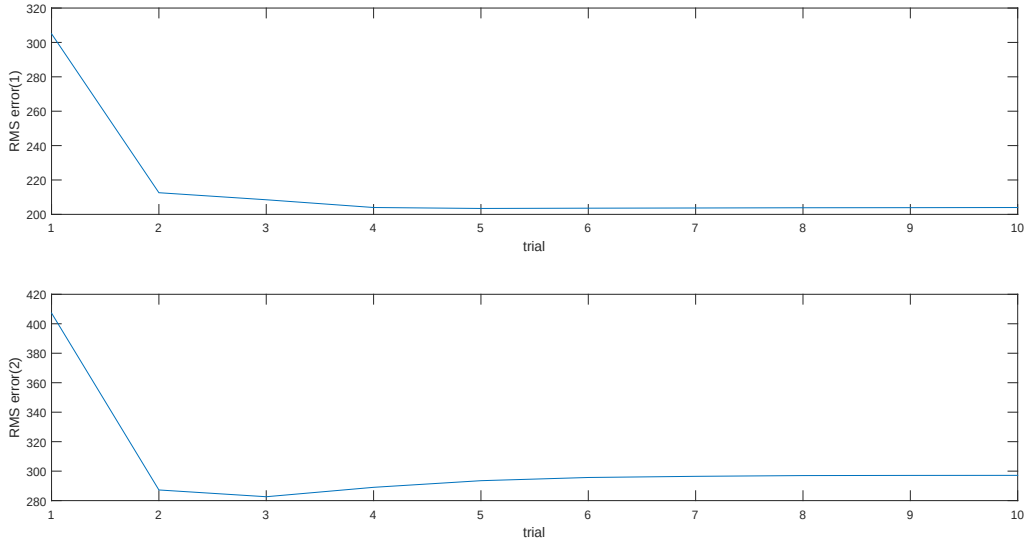

Figure 4.9: RMS error convergence for new set-point changes in 10 trials

Also, figure 4.10 illustrates improved set-point tracking performance of AVSC versus VSC after these 10 trials. Also, figure 4.11 illustrates MVs of AVSC versus VSC.

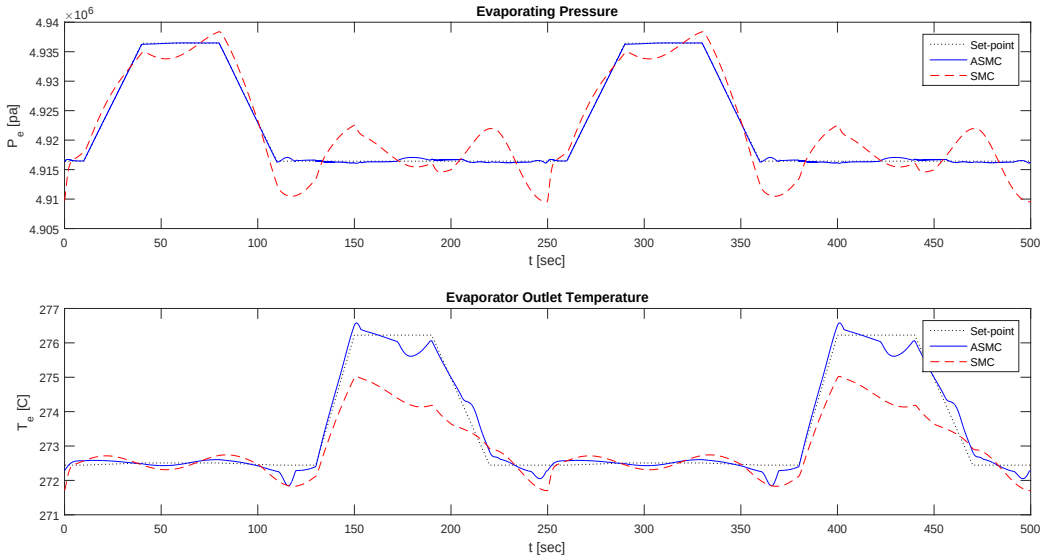

Figure 4.10: comparison of disturbance rejection performance between AVSC and VSC while tracking the set-point

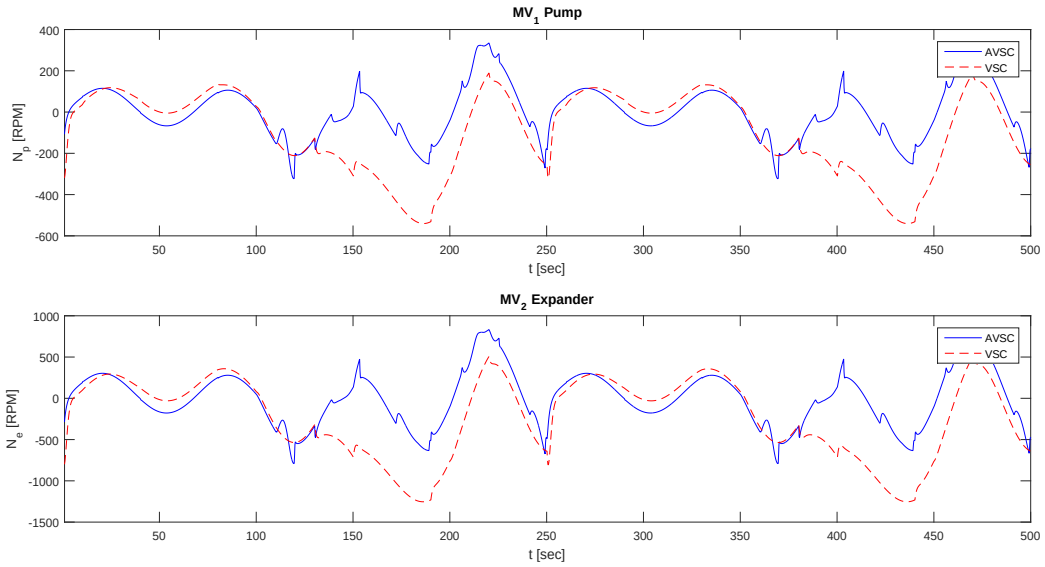

Figure 4.11: comparison of MVs between AVSC and VSC in set-point tracking

Similar to the previous test, CMAC neural networks outputs are shown in figure 4.12 where CMAC outputs is subtracted from the VSC term according to the control law.

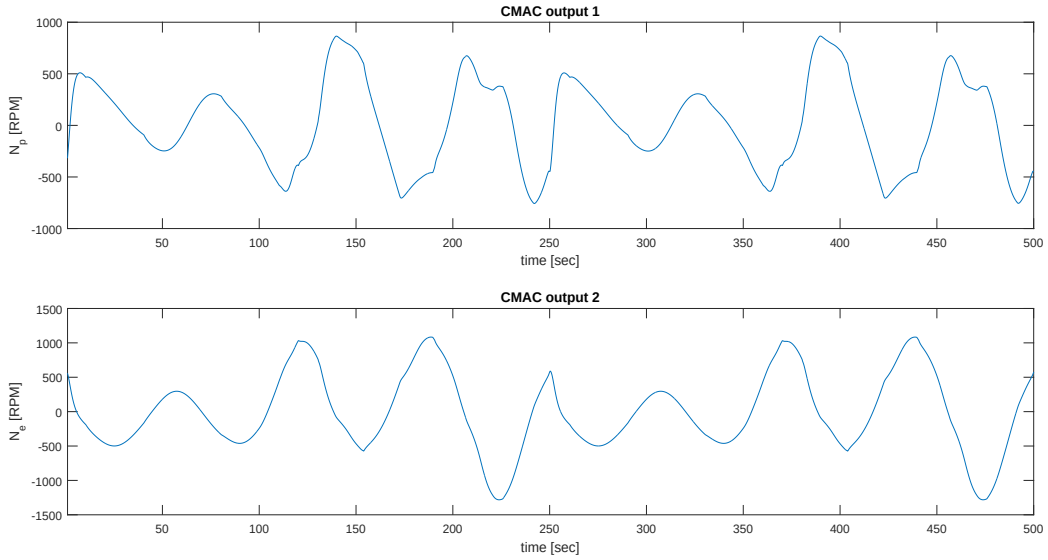

Figure 4.12: CMAC outputs

Finally, the sliding mode condition, $Hx = 0$, as a performance indicator is shown in figure 4.11 where the AVSC reveals smaller error than VSC in pressure channel.

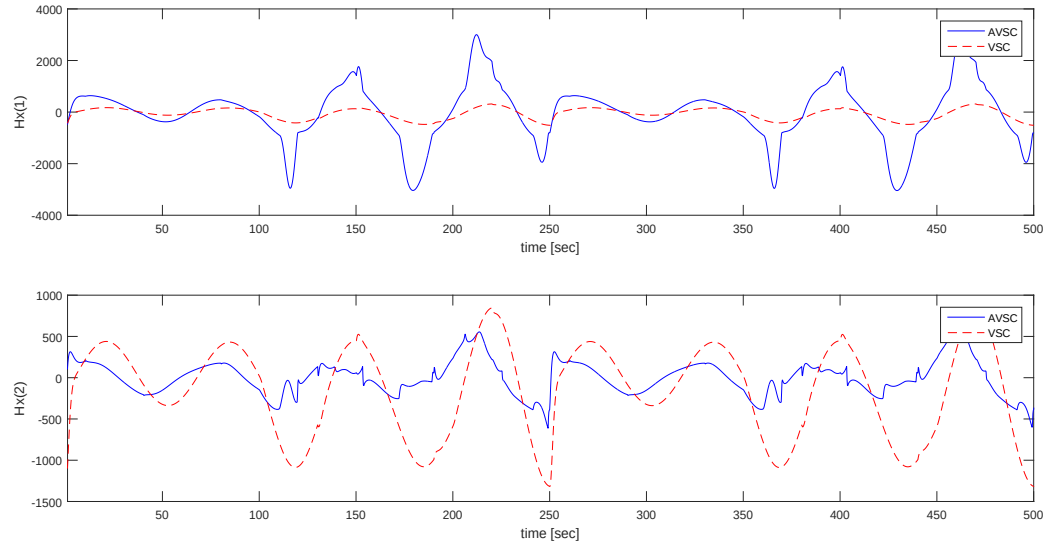

Figure 4.13: comparison of sliding mode performance between AVSC and VSC

4.2 Comparison with H_∞ Control

This section provides a brief introduction about H_∞ control synthesis and properties. H_∞ robust optimal control is one of the fundamental control strategies where it is an appropriate choice for TORC systems since significant uncertainties and disturbances are involved. Therefore, this control strategy is a fair choice for the sake of comparison with adaptive VSC.

In this work, H_∞ control is based on Glover and Doyle 1988 [53] and Doyle et al [54] such that a linear state space model is used for control synthesis. First, A state-space realization of the generalized plant can be formulated as below to cast H_∞ control,

$$\dot{x} = Ax + B_1 w + B_2 u \tag{4.2}$$

$$z = C_1 x + D_{11} w + D_{12} u \tag{4.3}$$

$$y = C_2 x + D_{21} w + D_{22} u \tag{4.4}$$

where w represents model uncertainties and disturbances in equation (4.2) whereas it represents white noise in (4.4). z error vector representing performance which should be minimized. y is the measurable output vector, and x is the state variable vector. Also, B_1 represents the defined uncertainty bounds of each dynamic equation and external disturbance, B_2 is the control input matrix, C_1 is constraints on state variables, C_2 is the output matrix.

H_∞ control is minimization of H_∞ norm of the closed-loop transfer function from w to z through stabilizing control, C_∞.

$$||G_{wz}||_\infty \equiv sup \left\{ \phi_{max} \left(G_{wz}(j\omega) \right) \right\} \tag{4.5}$$

where ϕ_{max} denoted maximum singular value. Moreover, there are some assumption typically made in H_∞ problems as follows:

1. The system is detectable and stabilizable,

2. D_{12} and D_{21} are full rank,

3. $D_{11} = 0$ and $D_{22} = 0$,

4. $D_{12}^T C_1 = 0$ and $B_1 D_{21}^T = 0$,

5. (A, B_1) is stabilizable and (A, C_1) is detectable.

Also,

$$D_{12} = \begin{bmatrix} 0 \\ I \end{bmatrix} \quad and \quad D_{21} = \begin{bmatrix} 0 & I \end{bmatrix}$$

are assumed being normalized. Now, the general H_∞ control which has the same order as the system (13^{th} order) is defined as below,

$$\dot{\hat{x}} = A_\infty + B_\infty (y - r) \tag{4.6}$$

$$u = C_\infty \hat{x} \tag{4.7}$$

Where,

$$B_\infty = -S_\infty C_2^T (I - \lambda^{-2} S_\infty P_\infty)^{-1},$$

$$C_\infty = -B_2^T P_\infty,$$

$$A_\infty = A + \lambda^{-2} B_1^T B_1 P_\infty + B_2 C_\infty + B_\infty C_2,$$

and λ is the value of H_∞ norm of closed-loop transfer function from z to w. λ is derived iteratively for all stabilizing control, H_∞, such that

$$||G_{wz}||_\infty < \lambda \tag{4.8}$$

Also, symmetric matrices, P_∞ and S_∞, are the solutions of Algebraic Riccati Equations (ARE) in the sense of H_∞ control structure,

$$A^T P_\infty + P_\infty A + C_1^T C_1 + P_\infty (\lambda^{-2} B_1^T B_1 - B_2 B_2^T) P_\infty = 0$$

Such that

$$Re\left\{\lambda_i(A+(\lambda^{-2}B_1^TB_1-B_2B_2^T)P_\infty)\right\}<0 \quad \forall i$$

and,

$$AS_\infty+S_\infty A^T+C_1^TC_1+S_\infty(\lambda^{-2}C_1^TC_1-C_2^TC_2)S_\infty=0$$

Such that,

$$Re\left\{\lambda_i(A+S_\infty(\lambda^{-2}C_1^TC_1-C_2^TC_2))\right\}<0 \quad \forall i.$$

It is noted that Hamiltonian matrix of this system has eigenvalues close to imaginary axis so that Schur method is used to solve two AREs [55, 56]. Finally, the controller is stabilizing if and only if $P_\infty>0$, $S_\infty>0$ satisfying AREs,

$$\rho(P_\infty S_\infty)<\lambda^2$$

Where, $\rho(\cdots)$ is an operator denoting the largest eigenvalue.

Recall that two crucial variables, evaporating pressure and evaporator outlet temperature, must be controlled concerning system performance and safety. Also, changes of pump rotation speed and turbine rotation speed are the control inputs, $u(t)$. According to the linearized model of TORC system, (4.2), (4.3) and (4.4), constraints on state variables are defined in matrix C_1. Also, the uncertainties and disturbance boundaries are determined in matrix B_1 so that the H_∞ controller (4.6)(4.7) is synthesized accordingly. To have a fair comparison, the performance indicator matrix, C_1, is determined according to the normalized cost function (3.27) in VSC design such that,

$$Q=C_1^TC_1.$$

Also, the uncertainties matrix, B_1, is determined according to the normalized cost function (3.71) in Kalman filter design such that,

$$Q_{est}=B_1B_1^T.$$

Finally, the time step is set to 0.1 seconds same as previous simulations. As a result shown in figure 4.14, the H_∞ controller can follow the set-point without any external disturbances.

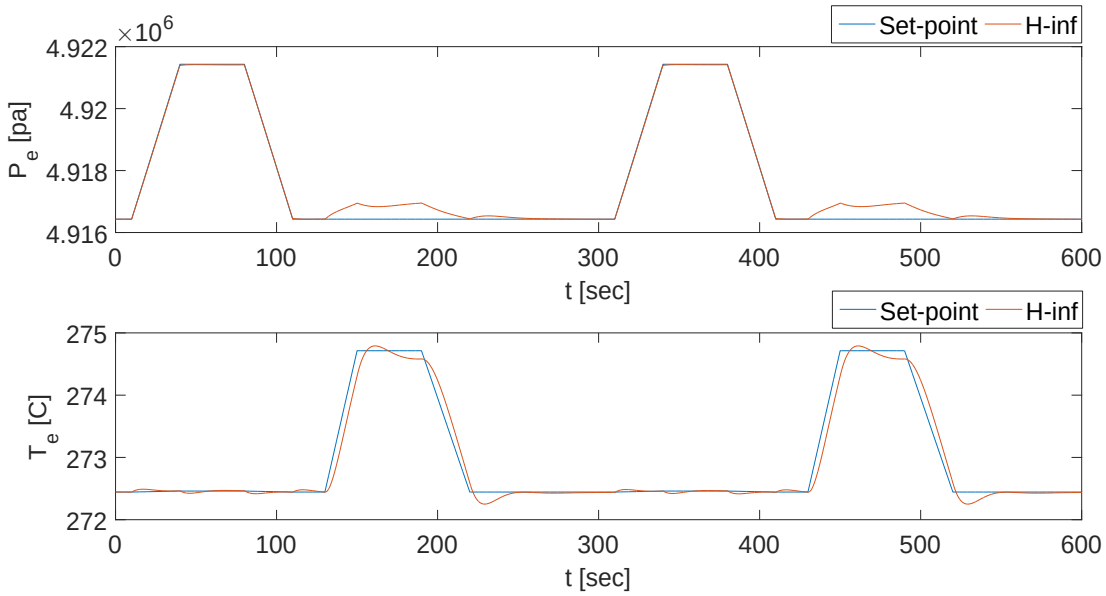

Figure 4.14: CVs of H_∞ control without disturbance

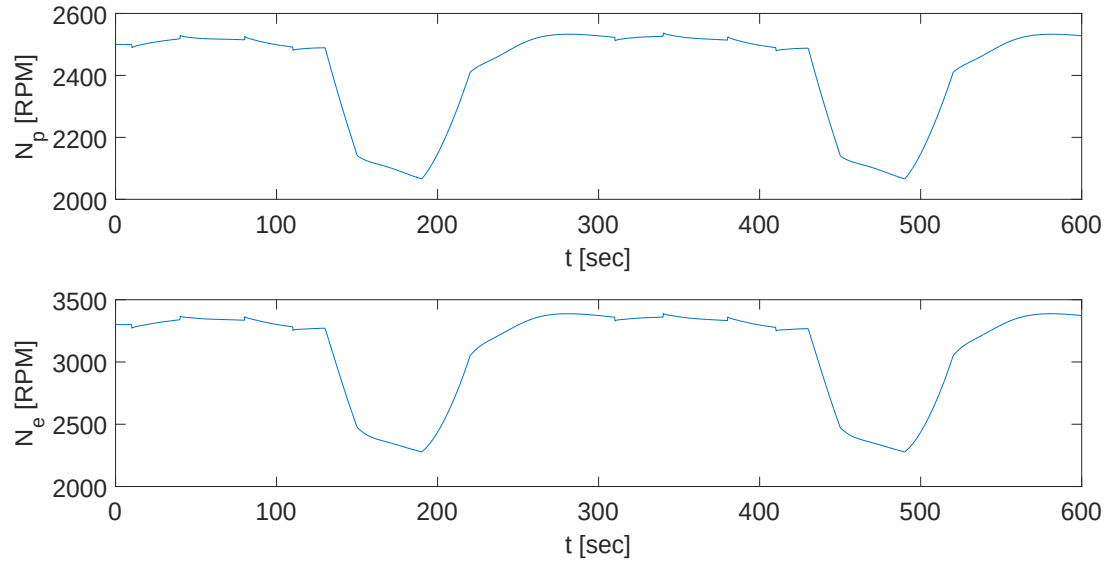

Figure 4.15: MVs of H_∞ control without disturbance

4.2.1 Disturbance Rejection Performance Comparison

Sine wave External disturbances in three different scenarios are imposed onto heat source temperature and heat source mass flow rate shown in figure 4.16. Then the disturbance rejection performance of AVSC after 50 trials is compared with H_∞ control. Figure 4.17 illustrates pressure and the outlet temperature of the evaporator as controlled variables in AVSC and H_∞ control while rejecting the imposed disturbances. As it is shown in the figure, the H_∞ control is not robust enough for this level of disturbance so that it does not show a satisfactory performance. On the other hand, AVSC can cancel out the effect of this disturbance and outperforms H_∞ control.

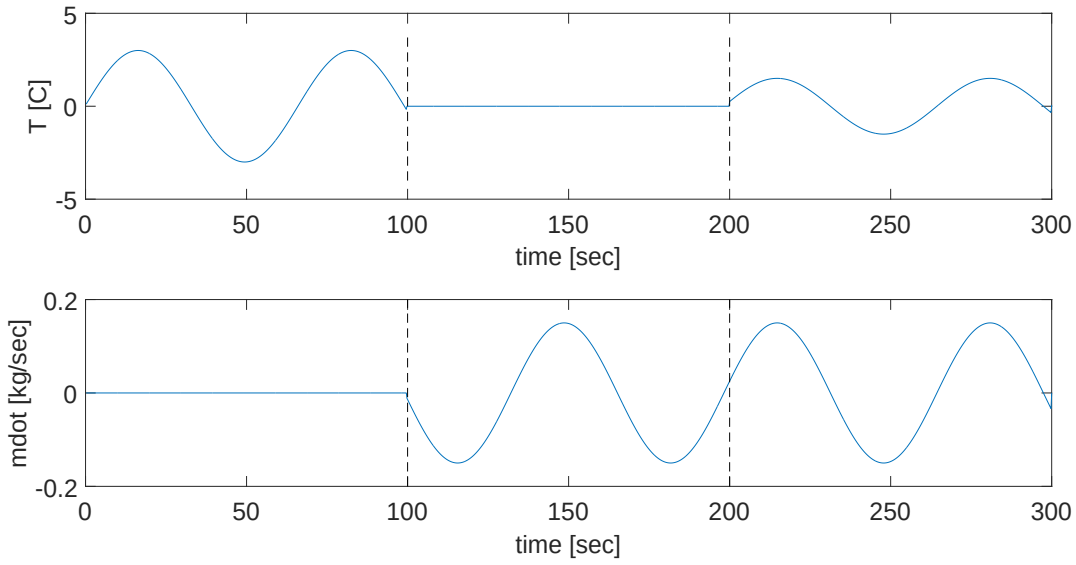

Figure 4.16: external disturbance on heat source temperature and mass flow rate

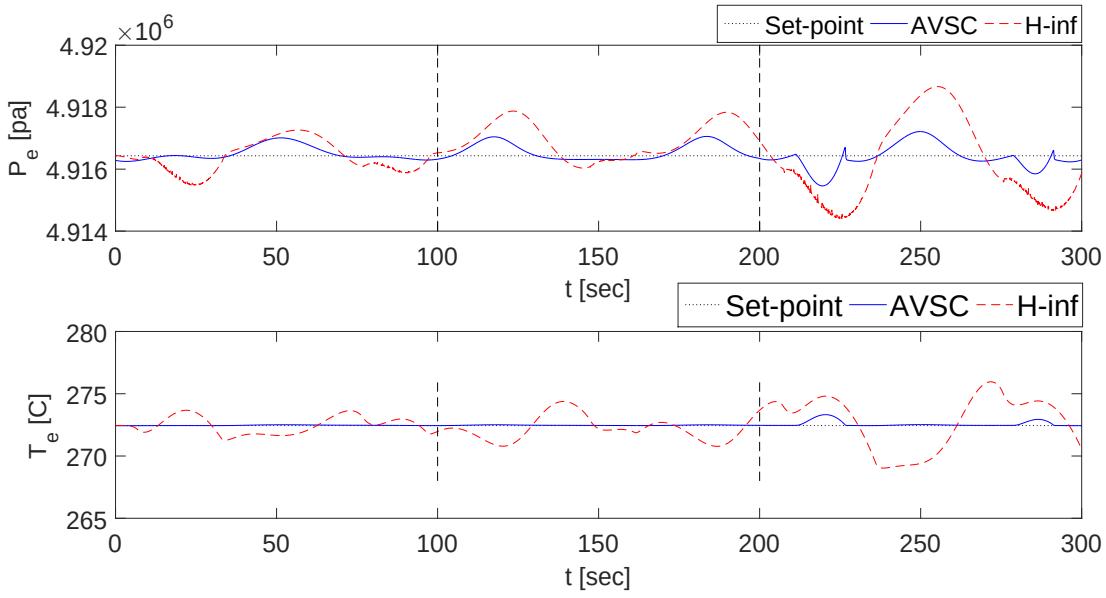

Figure 4.17: CVs of AVSC compared with H_∞ control while rejecting the disturbances

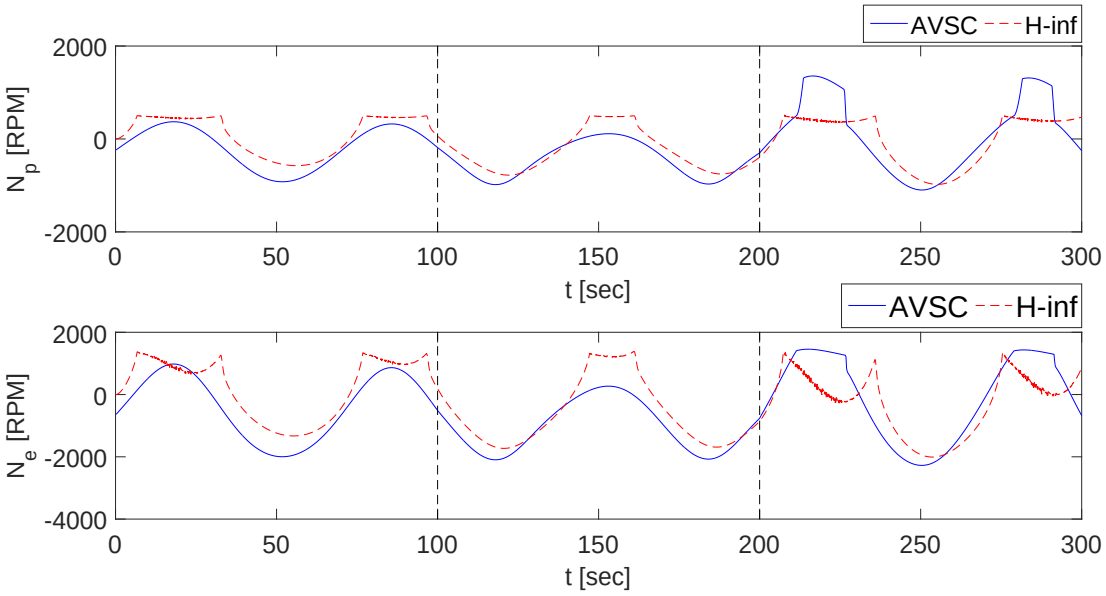

Figure 4.18: MVs of AVSC compared with H_∞ control while rejecting the disturbances

4.2.2 Set-point Tracking Performance Comparison

After comparing disturbance rejection performance in a constant operating condition, set-point tracking performance is also compared. This test compares the set-point tracking performance

while the same external disturbances shown in figure 4.16 are imposing into the system and the trained weight from the last test is used to initialize CMAC weights. Figure 4.19 illustrates the controlled variables, and figure 4.20 compares the manipulated variables where blue lines represent AVSC and red dashed lines represent H_∞ control. As it is shown in the figures, AVSC outperforms where blue lines represent AVSC and red dashed lines represent H_∞ control for these imposed disturbances.

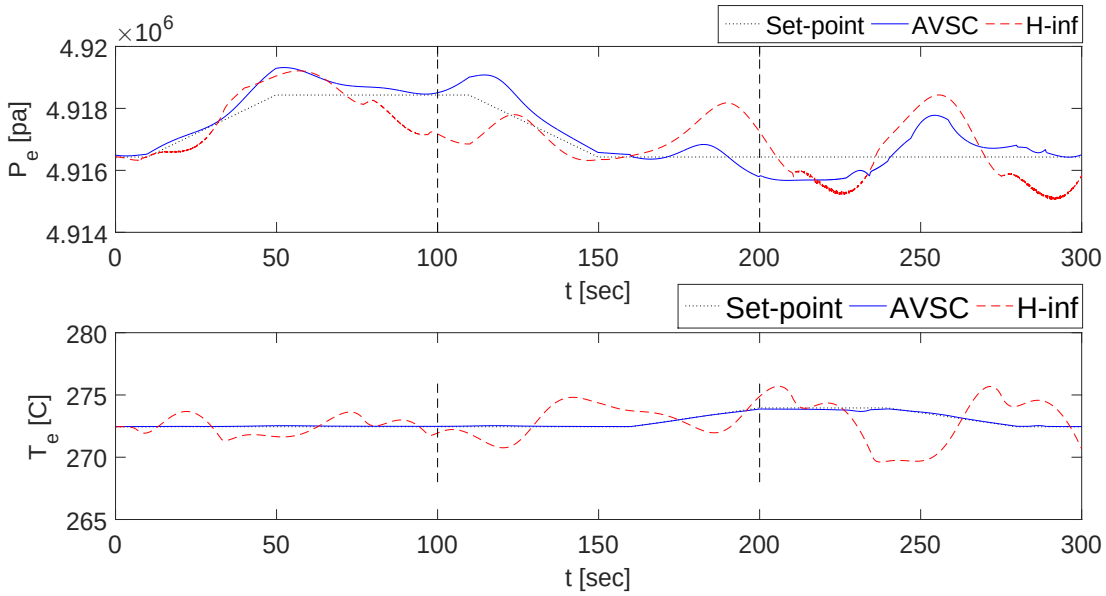

Figure 4.19: CVs of AVSC compared with H_∞ control in set-point tracking while rejecting the disturbances

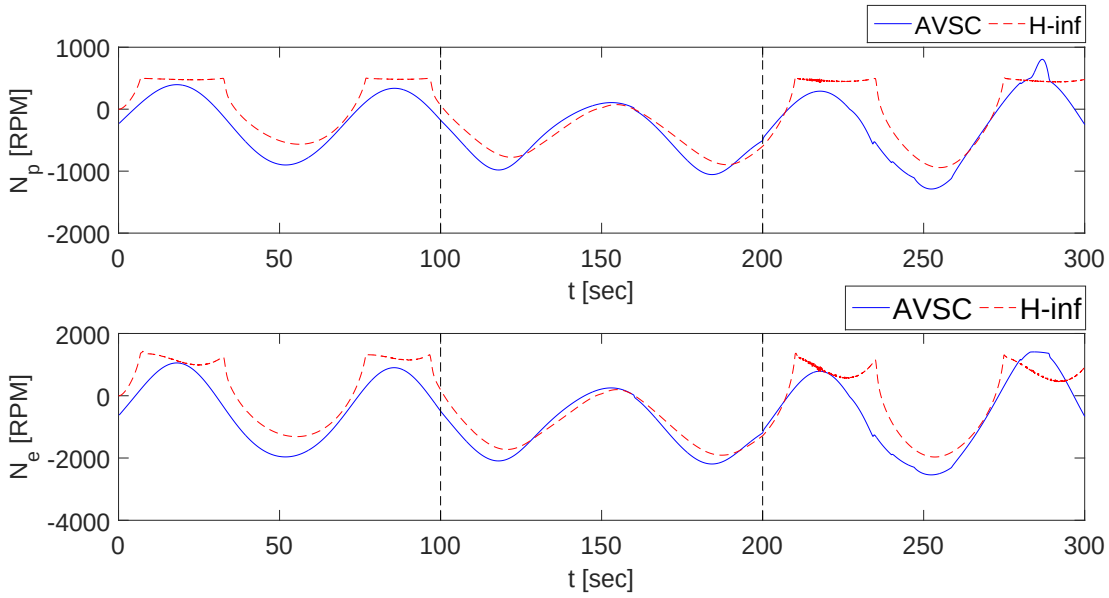

Figure 4.20: MVs of AVSC compared with H_∞ control in set-point tracking while rejecting the disturbances

4.3 Comparison with PI Control

This section compares the performance of AVSC with industrially accepted PI controls where the PI controls are tuned by IMC-PID tuning method [57]. In IMC tuning rule, two PI controllers are tuned for pressure and temperature channel where expander controls the pressure and pump controls the temperature [31]. The IMC method for second order processes is used to tune a PI controller for controlling the temperature channel,

$$\frac{T(s)}{U_{pp}(s)} = \frac{k_p}{(\tau_1 s+1)(\tau_2 s+1)} \tag{4.9}$$

Also, the IMC method for first order processes is used to tune another PI controller for controlling the pressure channel.

$$\frac{P(s)}{U_{exp}(s)} = \frac{k_p}{\tau s+1} \tag{4.10}$$

The transfer function corresponding to the PI control is as follows,

$$g_c(s) = k_c \frac{\tau_I s+1}{\tau_I s} \tag{4.11}$$

where for the second order process,

$$k_c = \frac{\tau_1 + \tau_2}{k_p \lambda} \quad , \quad \tau_I = \tau_1 + \tau_2 \tag{4.12}$$

And for the first order process,

$$k_c = \frac{\tau}{k_p \lambda} \quad , \quad \tau_I = \tau \tag{4.13}$$

where λ is the tuning parameter in IMC-tuning method. Figure 4.21 and 4.22 illustrate CVs and MVs where the tuned PI is controlling the closed-loop system without imposing external disturbances. According to the simulations, the PI controllers are well-tuned for controlling the plant.

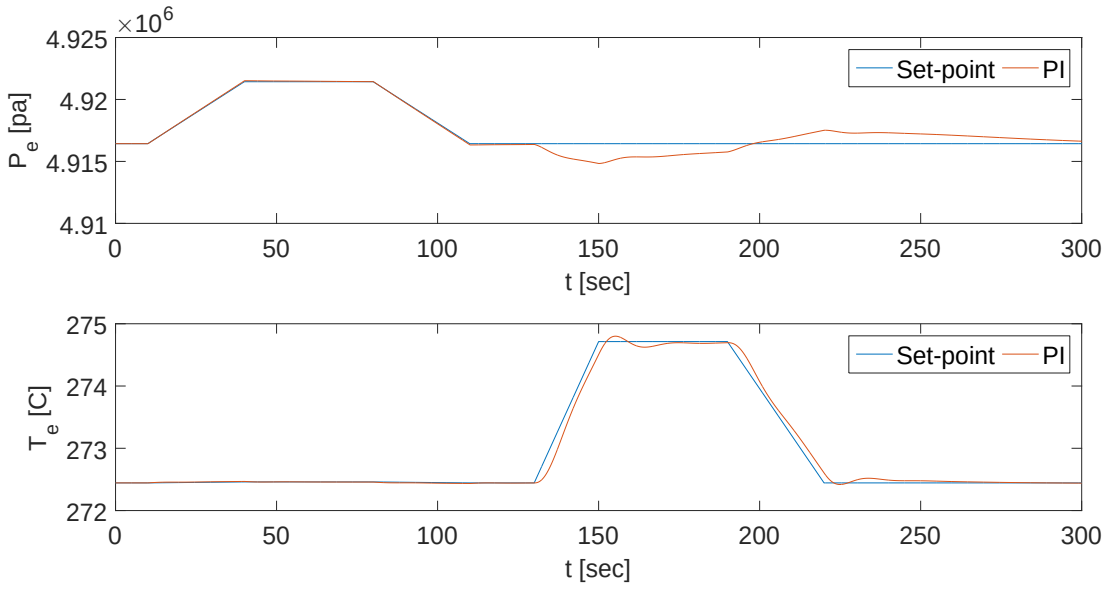

Figure 4.21: CVs of PI control without imposing external disturbances

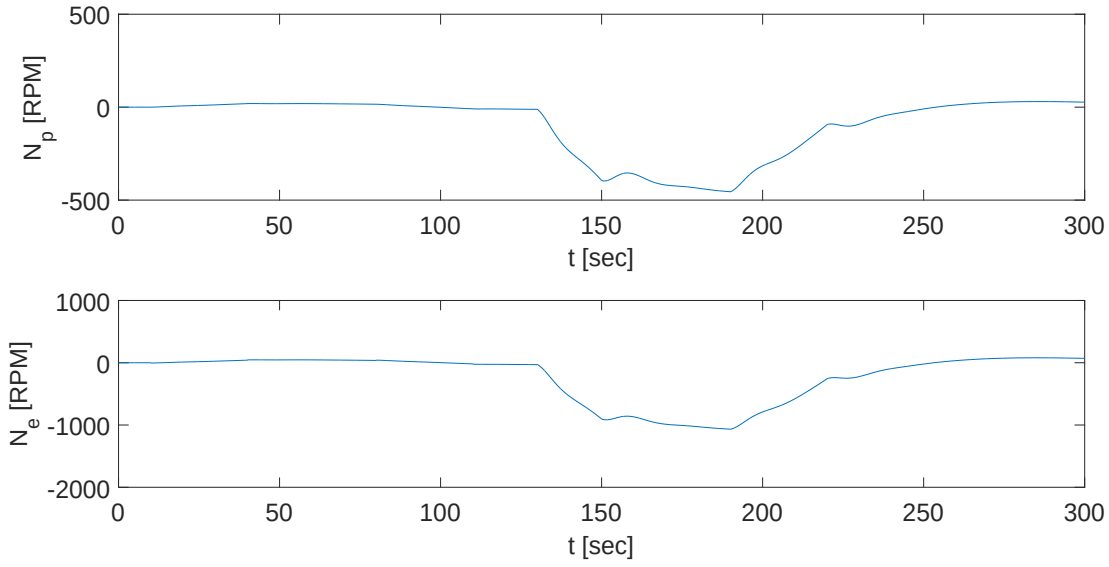

Figure 4.22: MVs of PI control without imposing external disturbances

4.3.1 Disturbance Rejection Performance Comparison

Sine wave External disturbances in three different scenarios are imposed onto heat source temperature and heat source mass flow rate shown in figure 4.16. Then the disturbance rejection performance of AVSC after 50 trials is compared with PI control. Figure 4.23 illustrates the CVs in AVSC and PI control while rejecting the imposed disturbances. As it is shown in the figure, AVSC can cancel out the effect of this disturbance and outperforms the PI control.

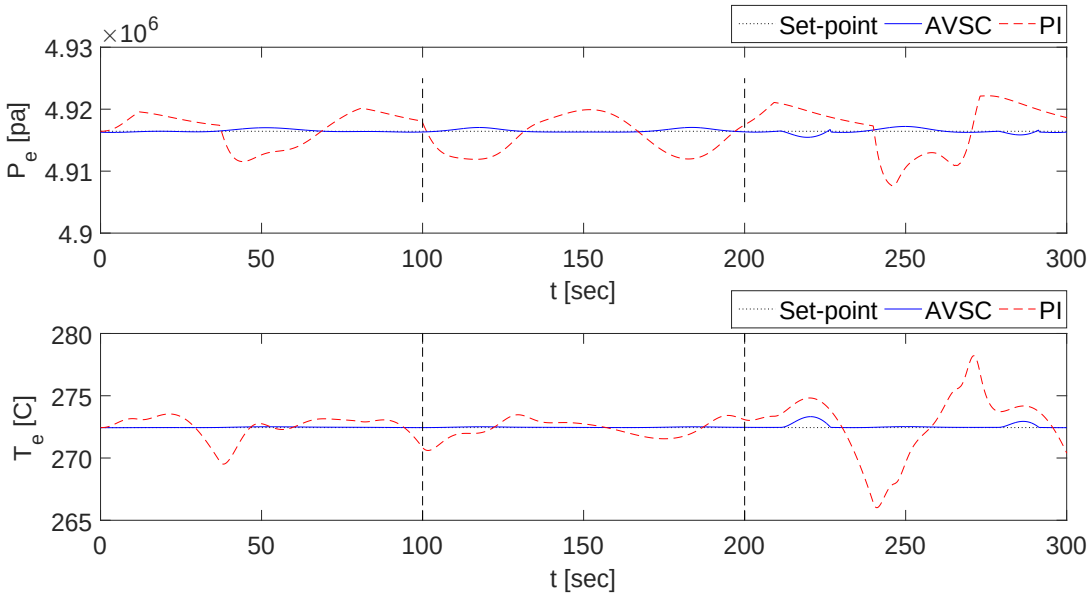

Figure 4.23: CVs of AVSC compared with PI control while rejecting the disturbances

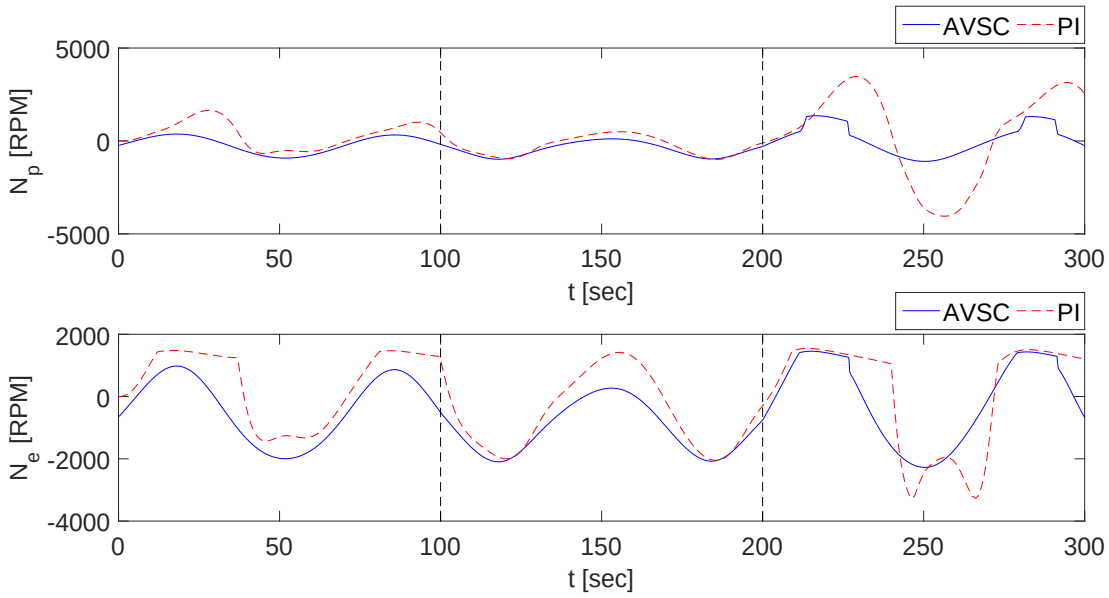

Figure 4.24: MVs of AVSC compared with PI control while rejecting the disturbances

4.3.2 Set-point Tracking Performance Comparison

After comparing disturbance rejection performance in a constant operating condition, set-point tracking performance is also compared. This test compares the set-point tracking performance

while the same external disturbances shown in figure 4.16 are imposing into the system and the trained weight from last test is used to initialize CMAC weights. Figure 4.25 illustrates the controlled variables, and figure 4.26 compares the CVs where blue lines represent AVSC and red dashed lines represent PI control. As it is shown in the figures, AVSC outperforms PI control in terms of set-point tracking and disturbance rejection.

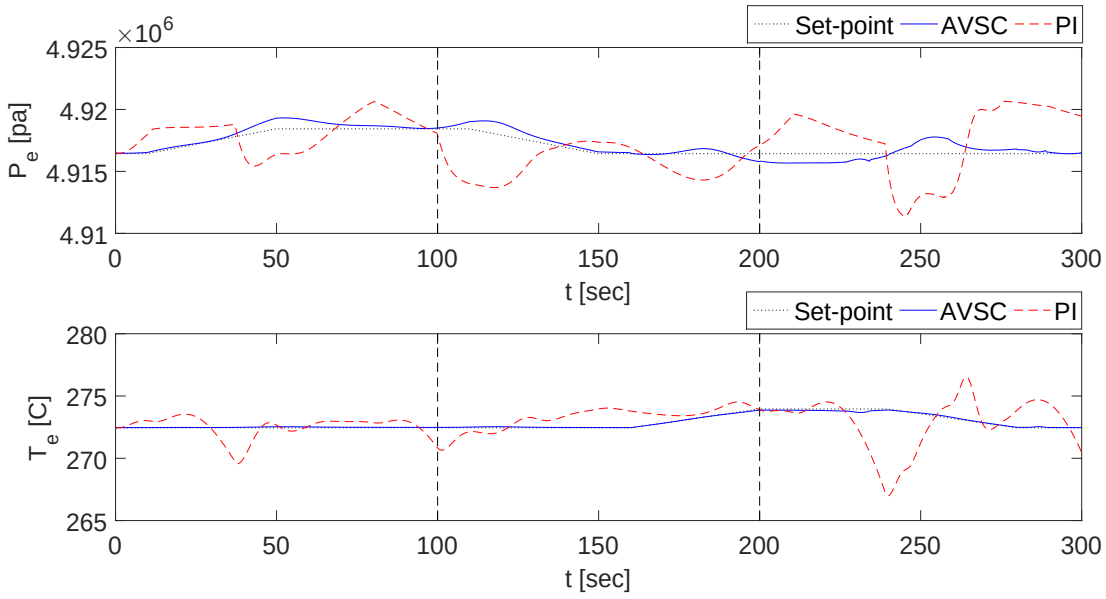

Figure 4.25: CVs of AVSC compared with PI control in set-point tracking while rejecting the disturbances

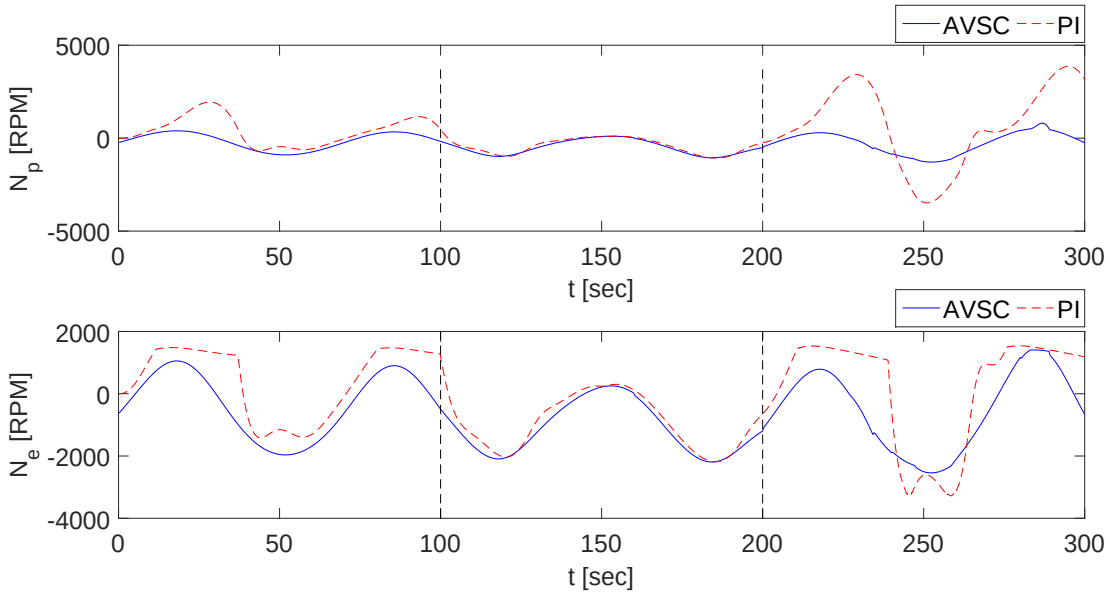

Figure 4.26: MVs of AVSC compared with PI control in set-point tracking while rejecting the disturbances

Chapter 5

CONCLUSION AND RECOMMENDATION

Disturbance rejection in TORC system resulted in performance optimization and net power output enhancement is an enabling key of co-generation systems. This thesis addressed such issue in TORC systems through a systematic process of control system design such that control-oriented model of TORC system was developed. Then, an adaptive robust optimal controller was designed such that the system could track optimal operating conditions while rejecting the disturbances to maximize the net power output. Moreover, the controller was effective despite model uncertainties since the controller was able to learn online through CMAC neural networks. Hence, the CMAC neural networks term canceled out the model nonlinearities, model uncertainties, and external disturbances.

5.1 Contributions

The aim of this thesis was to design an adaptive robust optimal control structure to mitigate the disturbances imposed by the heat source or model uncertainties. In this regards, the thesis approached the problem as follows:

- Due to lack of control-oriented models for TORC systems, a model was developed and proposed such that dynamic models of heat exchangers and semi-empirical static models of turbine expander and pump were derived due to slow dynamics of heat exchangers relative to fast dynamics of expander and pump. Therefore, MB-model for the condenser, a single region model for the evaporator and an LC-model for the recuperator constructed the dynamic model where the static model of the turbine expander and the pump were integrated into the dynamic model. In addition,

heat transfer coefficient of heat exchangers are calculated for single-phase and two-phase flow using a semi-empirical static correlation. Eventually, integration of all components' model built the final model of an SORC and a TORC.

- The controllability, observability, level of coupling among control inputs and control variables for the developed model were analyzed. Furthermore, the primary source of external disturbance to the TORC system and uncertainties were investigated such that rejection of them can improve the performance and enhance the net output power of TORC. Hence, addressing this problem leads us to determine control system design goal.

- Then, an optimal VSC as a robust control strategy was synthesized based on the developed model through developing an optimal hyperplane in the system state space where a quadratic cost function comprising state variable and control input constraints was minimized. Furthermore, a smoothing control technique was used to tackle chattering problem in VSC design such that a saturation function was selected as the robust term in the control law. Moreover, the stability of VSC was analyzed based on Lyapunov stability theory where it was shown that the control system was asymptotically stable. To improve robustness margin of the VSC design, CMAC neural network method was integrated into the VSC to make the control system adaptive to the disturbances and uncertainties.

- CMAC neural network due to fast adaptability and low computational burden was selected as a proper choice such that it was trained online by partial system state. The adaptive rule or weight update law was derived based on Lyapunov stability theory where a quadratic Lyapunov function representing energy elements of the system was introduced where the quadratic term of the optimal hyperplane and the quadratic term of the CMAC weight error constructed the Lyapunov function. According to Lyapunov theory, the proposed Lyapunov function must be dissipative

as time goes by to guarantee the stability of the system. Therefore, the adaptive rule was derived such that it makes time derivative of the Lyapunov function semi-negative definite which means the control system is Uniformly Ultimately Bounded (UUB).

- Also, to estimate unmeasurable state variables and filter out measurement noises, a Kalman filter was utilized to design an optimal state observer. Then, the observed state fed the adaptive VSC design to improve the practicality aspect. To the extent of our knowledge, there is no stability proof for integration of an observer into the control system so far, and it has been a well-known problem in control system area. Hence the observer design left without stability analysis.

- Ultimately, the proposed control is not only suitable for TORC application but also provides a methodology for the class of uncertain systems.

.

5.2 Recommendations and Future Work

The next step of this research work may be to examine the performance of the proposed adaptive VSC on a physical set-up. CMAC neural network has already been tested on a robotic arm where it shows effective control performance in case of model uncertainties and external disturbances. Also, modern computer technology has made real-time utilization of CMAC neural network with quite a few of inputs viable.

As a future frontier of this research work, the heat source can be studied and modeled so that considering the heat source dynamics may improve the robustness margin of the control system. For instance, in this application, the heat source is a secondary cycle where the mass flow rate of its working fluid can be controlled by a pump.

Bibliography

[1] T. E. Commission, "2050 low-carbon economy."

[2] Alberta Government, "Climate Leadership."

[3] ABB, "Power Generation Energy Efficient Design of Auxiliary Systems in Fossil-Fuel Power Plants," p. 358, 2009.

[4] Y. A. Cengel and M. A. Boles, *Thermodynamics : an engineering approach*. New York: McGraw-Hill, 2011.

[5] T. C. Hung, T. Y. Shai, and S. K. Wang, "A review of organic rankine cycles (ORCs) for the recovery of low-grade waste heat," *Energy*, vol. 22, no. 7, pp. 661–667, 1997.

[6] B. F. Tchanche, G. Lambrinos, A. Frangoudakis, and G. Papadakis, "Low-grade heat conversion into power using organic Rankine cycles - A review of various applications," *Renewable and Sustainable Energy Reviews*, vol. 15, no. 8, pp. 3963–3979, 2011.

[7] Z. Shengjun, W. Huaixin, and G. Tao, "Performance comparison and parametric optimization of subcritical Organic Rankine Cycle (ORC) and transcritical power cycle system for low-temperature geothermal power generation," *Applied Energy*, vol. 88, pp. 2740–2754, aug 2011.

[8] U. Drescher and D. Brüggemann, "Fluid selection for the Organic Rankine Cycle (ORC) in biomass power and heat plants," *Applied Thermal Engineering*, vol. 27, pp. 223–228, jan 2007.

[9] H. Gao, C. Liu, C. He, X. Xu, S. Wu, and Y. Li, "Performance analysis and working fluid selection of a supercritical organic rankine cycle for low grade waste heat recovery," *Energies*, vol. 5, no. 9, pp. 3233–3247, 2012.

[10] A. I. Papadopoulos, M. Stijepovic, and P. Linke, "On the systematic design and selection of optimal working fluids for Organic Rankine Cycles," *Applied Thermal Engineering*, vol. 30, pp. 760–769, may 2010.

[11] J. Li, G. Pei, Y. Li, and J. Ji, "Evaluation of external heat loss from a small-scale expander used in organic Rankine cycle," *Applied Thermal Engineering*, vol. 31, pp. 2694–2701, oct 2011.

[12] G. Qiu, H. Liu, and S. Riffat, "Expanders for micro-CHP systems with organic Rankine cycle," *Applied Thermal Engineering*, vol. 31, pp. 3301–3307, nov 2011.

[13] N. B. Desai and S. Bandyopadhyay, "Process integration of organic Rankine cycle," *Energy*, vol. 34, pp. 1674–1686, oct 2009.

[14] C. Vetter and H.-j. Wiemer, "Dynamic Simulation of a Supercritical ORC Using Low-Temperature Geothermal Heat," no. April, pp. 19–25, 2015.

[15] B. Twomey, P. A. Jacobs, and H. Gurgenci, "Dynamic performance estimation of small-scale solar cogeneration with an organic Rankine cycle using a scroll expander," *Applied Thermal Engineering*, vol. 51, no. 1-2, pp. 1307–1316, 2013.

[16] T. Endo, S. Kawajiri, Y. Kojima, K. Takahashi, T. Baba, S. Ibaraki, T. Takahashi, and M. Shinohara, "Study on Maximizing Exergy in Automotive Engines," in *SAE Technical Paper*, SAE International, 2007.

[17] S. Skogestad and I. Postlethwaite, *Multivariable feedback control: analysis and design*, vol. 8. John Wiley & Sons, second ed., 2001.

[18] M. Siguard Skogestad, Morari and J. C. Doyles, "Robust Control of Ill-Conditioned Plants: High-Purity Distillation," *IEEE Transactions on Automatic Control*, vol. 33, no. 12, pp. 1092–1105, 1988.

[19] J. Zhang, W. Zhang, G. Hou, and F. Fang, "Dynamic modeling and multivariable control of organic Rankine cycles in waste heat utilizing processes," *Computers and Mathematics with Applications*, vol. 64, no. 5, pp. 908–921, 2012.

[20] J. Zhang, Y. Zhou, R. Wang, J. Xu, and F. Fang, "Modeling and constrained multivariable predictive control for ORC (Organic Rankine Cycle) based waste heat energy conversion systems," *Energy*, vol. 66, pp. 128–138, 2014.

[21] D. Wei, X. Lu, Z. Lu, and J. Gu, "Dynamic modeling and simulation of an Organic Rankine Cycle (ORC) system for waste heat recovery," *Applied Thermal Engineering*, vol. 28, no. 10, pp. 1216–1224, 2008.

[22] J. M. Jensen and H. Tummescheit, "Moving Boundary Models for Dynamic Simulations of Two-Phase Flows," in *2nd International Modelica Conference*, vol. 3, pp. 235–244, 2002.

[23] J. M. Jensen, *Dynamic Modeling of Thermo-Fluid Systems With focus on evaporators*. PhD thesis, 2003.

[24] X.-D. He, S. Liu, and H. H. Asada, "Modeling of Vapor Compression Cycles for Multivariable Feedback Control of HVAC Systems," *Journal of Dynamic Systems, Measurement, and Control*, vol. 119, no. 2, p. 183, 1997.

[25] X.-D. He, S. Liu, H. Asada, and H. Itoh, "Multivariable Control of Vapor Compression Systems," *HVAC&R Research*, vol. 4, no. 3, pp. 205–230, 1998.

[26] B. P. Rasmussen, A. G. Alleyne, and A. B. Musser, "Model-driven system identification of transcritical vapor compression systems," *IEEE Transactions on Control Systems Technology*, vol. 13, no. 3, pp. 444–451, 2005.

[27] D. Luong and T.-c. Tsao, "Linear Quadratic Integral Control of an Organic Rankine Cycle for Waste Heat Recovery in Heavy-Duty Diesel Powertrain," pp. 3147–3152, 2014.

[28] M. C. Esposito, N. Pompini, A. Gambarotta, V. Chandrasekaran, J. Zhou, and M. Canova, "Nonlinear Model Predictive Control of an Organic Rankine Cycle for Exhaust Waste Heat Recovery in Automotive Engines," *IFAC-PapersOnLine*, vol. 48, no. 15, pp. 411–418, 2015.

[29] F. P. Incropera, *Fundamentals of Heat and Mass Transfer*. John Wiley & Sons, 2006.

[30] S. Quoilin, V. Lemort, and J. Lebrun, "Experimental study and modeling of an Organic Rankine Cycle using scroll expander," *Applied Energy*, vol. 87, no. 4, pp. 1260–1268, 2010.

[31] S. Quoilin, R. Aumann, A. Grill, A. Schuster, V. Lemort, and H. Spliethoff, "Dynamic modeling and optimal control strategy of waste heat recovery Organic Rankine Cycles," *Applied Energy*, vol. 88, no. 6, pp. 2183–2190, 2011.

[32] J. Zhang, J. Feng, Y. Zhou, F. Fang, and H. Yue, "Linear Active Disturbance Rejection Control of Waste Heat Recovery Systems with Organic Rankine Cycles," pp. 5111–5125, 2012.

[33] J. Zhang, Y. Zhou, Y. Li, G. Hou, and F. Fang, "Generalized predictive control applied in waste heat recovery power plants," *Applied Energy*, vol. 102, pp. 320–326, 2013.

[34] G. Hou, S. Bi, M. Lin, J. Zhang, and J. Xu, "Minimum variance control of organic Rankine cycle based waste heat recovery," *Energy Conversion and Management*, vol. 86, pp. 576–586, oct 2014.

[35] R. E. Kalman, "A New Approach to Linear Filtering and Prediction Problems," *Journal of Basic Engineering*, vol. 82, no. 1, p. 35, 1960.

[36] J. Pettersen, R. Rieberer, and S. T. Munkejord, "HEAT TRANSFER AND PRESSURE DROP FOR FLOW OF SUPERCRITICAL AND SUBCRITICAL C0 2 IN MICROCHANNEL TUBES by DTIC QUALITY IN ˆ BGMSD 4," *Refrigeration And Air Conditioning*, 2000.

[37] R. DeCarlo, S. Zak, and G. Matthews, "Variable Structure Control of Nonlinear Multivariable Systems : A Tutorial," *In Proceedings of the IEEE*, vol. 76, no. 3, pp. 212–232, 1988.

[38] V. Utkin, "Variable structure systems with sliding modes," *IEEE Transactions on Automatic Control*, vol. 22, no. 2, pp. 212–222, 1977.

[39] C. Dorling and A. Zinober, "Two approaches to hyperplane design in multivariable variable structure control systems," *International Journal of Control*, vol. 7179, no. April, 1986.

[40] Jeff K Pieper, "First Order Dynamic Sliding Mode Control," in *Proceedings of the 37th IEEE Conference on Decision & Control , Tampa, Florida USA December 1998*, no. 2, pp. 155–157, 1998.

[41] Utkin, "All Russian mathematical portal," vol. 8, no. 3, pp. 33–165, 1978.

[42] J. X, B. W. Surgenor, and J. Pieper, "Optimal Discrete Sliding Mode Control with Application," 1992.

[43] Y. Kim, F. Lewis, and D. Dawson, "Intelligent optimal control of robotic manipulators using neural networks," *Automatica*, vol. 36, pp. 1355–1364, 2000.

[44] M. Abu-Khalaf and F. L. Lewis, "Nearly optimal control laws for nonlinear systems with saturating actuators using a neural network HJB approach," *Automatica*, vol. 41, no. 5, pp. 779–791, 2005.

[45] D. Vrabie and F. L. Lewis, "Adaptive Optimal Control Algorithm for Continuous-Time Nonlinear Systems Based on Policy Iteration," pp. 73–79, 2008.

[46] Z. Chen and S. Jagannathan, "Generalized hamilton-jacobi-bellman formulation -based neural network control of affine nonlinear discrete-time systems.," *IEEE transactions on neural networks / a publication of the IEEE Neural Networks Council*, vol. 19, no. 1, pp. 90–106, 2008.

[47] P. Medagam and F. Pourboghrat, "Optimal control of nonlinear systems using RBF neural network and adaptive extended Kalman filter," *2009 American Control Conference*, pp. 355–360, 2009.

[48] N. Al-Holou, T. Lahdhiri, J. Weaver, and F. Al-Abbas, "Sliding mode neural network inference fuzzy logic control for active suspension systems," *IEEE Transactions on Fuzzy Systems*, vol. 10, no. 2, pp. 234–246, 2002.

[49] J. Albus, "A new approach to manipulator control: The cerebellar model articulation controller (CMAC)," *Journal of Dynamic Systems, Measurement, and Control*, no. SEPTEMBER, pp. 220–227, 1975.

[50] A. Taghavipour, M. S. Foumani, and M. Boroushaki, "Implementation of an optimal control strategy for a hydraulic hybrid vehicle using CMAC and RBF networks," *Scientia Iranica*, vol. 19, no. 2, pp. 327–334, 2012.

[51] R. M. Kretchmar and C. W. Anderson, "Comparison of CMACs and radial basis functions for local function approximators in reinforcement learning," *Neural Networks,1997., International Conference on*, vol. 2, pp. 834–837 vol.2, 1997.

[52] C. J. B. Macnab, "Preventing bursting in approximate-adaptive control when using local basis functions," *Fuzzy Sets and Systems*, vol. 160, no. 4, pp. 439–462, 2009.

[53] K. Glover and J. C. Doyle, "State-space formulae for all stabilizing controllers that satisfy an H???-norm bound and relations to relations to risk sensitivity," *Systems and Control Letters*, vol. 11, no. 3, pp. 167–172, 1988.

[54] J. Doyle, K. Glover, P. Khargonekar, and B. Francis, "State-space solutions to standard H/sub 2/ and H/sub infinity / control problems," *IEEE Transactions on Automatic Control*, vol. 34, no. 8, pp. 831–847, 1989.

[55] A. Laub, "A Schur method for solving algebraic Riccati equations," *IEEE Transactions on Automatic Control*, vol. 24, no. 6, pp. 913–921, 1979.

[56] V. B. Larin, "Algorithm for solving algebraic Riccati equation which has singular Hamiltonian matrix," *Systems & Control Letters*, vol. 36, pp. 231–239, 1999.

[57] S. Skogestad, “Probably the best simple PID tuning rules in the world,” *Journal of Process Control*, pp. 1–27, 2001.